FAMOSS, a conserved 41-aa peptide involved in plant tip growth regulation

Anna Mamaeva[1,*], Andrey Kniazev[1], Ilia Sedlov[1], Nina Golub[1], Daria Kharlampieva[2], Valentin Manuvera[2], Victor Rakitin[3], Alexander Nosov[3], Artem Fomenkov[3], Marat Pavlyukov[1], Sergey Kovalchuk[1], Rustam Ziganshin[1], Anna Glushkevich[1], Vassili Lazarev[2,4], and Igor Fesenko[1]

[1] The Laboratory of functional genomics and plant proteomics, Shemyakin and Ovchinnikov Institute of Bioorganic Chemistry of the Russian Academy of Sciences, Moscow, 117997, Russian Federation;

[2] Department of Cell Biology, Federal Research and Clinical Center of Physical-Chemical Medicine of Federal Medical Biological Agency, Moscow, 119435, Russian Federation;

[3] Timiryazev Institute of Plant Physiology, Russian Academy of Sciences, 127276 Moscow, Russian Federation;

[4] Moscow Institute of Physics and Technology (National Research University), Dolgoprudny, Moscow region, 141701, Russian Federation.

Correspondence: [*] Anna Mamaeva (AnnetteSt@yandex.ru)
Running Title: lncRNA-encoded peptide regulates plant growth

Abstract

Recent evidence shows that small open reading frame (smORF; <100 codons)-encoded peptides (SEPs) containing transmembrane domains are preadapted to be progenitors of novel functional genes. A dozen of such SEPs translated from long non-coding RNAs (lncRNAs) are already functionally characterised in animals. However, functional plant lncRNA-smORF-coded peptides are not yet described. Here, we report detailed functional characterization of a 41-aa peptide encoded by lncRNA-smORFs in the moss Physcomitrium patens, which was named "FAst-growing MOSS" (FAMOSS). We found that the FAMOSS interacts with the Rab-type small GTPase proteins and its overexpression leads to faster moss growth rate and more intensive vesicular transport in apical cells, while its knockout results in the opposite effect. The FAMOSS contains a predicted transmembrane domain and possible orthologs from streptophyta algae to flowering plants have a very conserved structure. Thus, the FAMOSS peptide is a

33   previously unknown conserved player of Rab-mediated processes in plants. Our findings are in

34   line with functional studies of transmembrane SEPs in animals and prove the principles of SEPs

35   evolution. This study provides new insights into functions of plant lncRNA-smORFs.

36   **Keywords:** peptide encoded by lncRNA-smORF, *Physcomitrium patens,* vesicular

37   trafficking

Introduction

39   Eukaryotic transcriptomes contain numerous RNAs with low coding potential (non-coding

40   RNAs), including long non-coding RNAs (lncRNAs), primary microRNAs (pri-miRNA), and

41   circular RNAs (circRNAs) (Li et al., 2017). LncRNAs are transcripts longer than 200

42   nucleotides that contain only small open reading frames (smORFs; <100 codons) and are

43   unlikely to encode functional proteins. Despite this definition, several functional peptides and

44   microproteins have recently been shown to be encoded by smORFs in mice (Anderson et al.,

45   2015), humans (D'Lima et al., 2017; Huang et al., 2017; Slavoff et al., 2014), zebrafish (Chng et

46   al., 2013), fruit flies (Immarigeon et al., 2021; Magny et al., 2013), *Arabidopsis thaliana*

47   (Hanada et al., 2013), and the moss *Physcomitrium* (previously *Physcomitrella*) *patens* (Fesenko

48   et al., 2019). These smORF-encoded peptides (SEPs) are involved in the regulation of cell

49   proliferation (Polycarpou-Schwarz et al., 2018), cancer growth (Guo et al., 2020; Huang *et al.*,

50   2017), apoptosis and autophagosome formation (Rubtsova et al., 2018), mitochondrial

51   respiratory chain activity (Chugunova et al., 2019), muscle function (Matsumoto et al., 2017),

52   antigen presentation (Niu et al., 2020), heart development (Chng *et al.*, 2013), and sexual

53   reproduction (Immarigeon *et al.*, 2021). Unlike for animals, only a few examples of functional

54   SEPs have been described in plants. They have been shown to regulate plant programmed cell

55   death (Blanvillain et al., 2011), root growth and development (Casson et al., 2002; Chen et al.,

56   2020), cell proliferation and expansion (Brito et al., 2018; Ikeuchi et al., 2011), nodule formation

57   (Rohrig et al., 2002), and pollen germination (Dong et al., 2013).

58   Because of their small size, smORFs do not contain functional domains or may include

59   only simple ones, such as a transmembrane α-helix. Indeed, a "transmembrane-first" model of

60   gene birth suggests that peptides with a transmembrane domain may accidently appear in

61   thymine-rich non-genic regions (Vakirlis et al., 2020). A pool of uncharacterized SEPs located

62   at, and interacting with, cellular membranes was detected in different studies; for example, the

63   56-aa Mtln peptide interacts with NADH-dependent cytochrome b5 reductase (Chugunova *et al.*,

64   2019), the 90-aa SPAR peptide interacts with V-ATPase (Matsumoto *et al.*, 2017), and the 28-aa

65   Sarcolamban A interacts with Sarco-endoplasmic Reticulum Ca^{2+} adenosine triphosphatase

2

66   (SERCA) (Magny *et al.*, 2013). The identification of protein partners of the SEPs helps elucidate

67   their functions (Matsumoto *et al.*, 2017; Slavoff *et al.*, 2014); for example, a human 7-kDa

68   microprotein, NoBody, binds the mRNA decapping complex to regulate the number of P-bodies

69   in a cell (D'Lima *et al.*, 2017). The 10-kDa microprotein CASIMO1 controls cell proliferation by

70   interacting with squalene epoxidase that is a key enzyme in cholesterol synthesis and a known

71   oncogene in breast cancer (Polycarpou-Schwarz *et al.*, 2018).

72   Previously, we identified functional smORFs encoded by lncRNAs in the model plant

73   *Physcomitrium patens*, a moss (Fesenko *et al.*, 2019). The knockout of four selected SEPs,

74   PSEP1, PSEP3, PSEP18, and PSEP25, resulted in significantly reduced growth rates in the moss

75   protonemata (Fesenko *et al.*, 2019). In this study, we investigated the functions of PSEP1, which

76   was renamed the FAst-growing MOSS (FAMOSS) peptide. We demonstrated that this SEP

77   participates in the regulation of polar tip growth in *P. patens* via its interaction with Rab-type

78   small GTPases. We observed that mutant plants lacking FAMOSS had altered apex-derived

79   vesicular trafficking and different protonemal filament structures compared with the wild type.

80   Our quantitative proteomic analysis revealed a downregulation of the stress-responsive proteins

81   in both the *FAMOSS*-overexpressing (OE) and knockout (KO) lines, as well as an altered

82   sensitivity to phytohormones. Finally, we proposed that the FAMOSS peptide is a novel

83   component of the Rab protein complexes that regulate vesicular trafficking and stress responses

84   in plants.

85

Results

FAMOSS is widely distributed across different plant lineages

88   Recently, we used a combined approach to identify functional SEPs encoded by lncRNAs

89   in the model plant *P. patens* (Fesenko *et al.*, 2019). In this analysis, we identified the 41-aa

90   peptide PSEP1 (Physcomitrella smORF-encoded peptide 1), encoded by the transcript

91   CNT2064811, which was predicted to be a non-coding RNA in the CANTATAdb database

92   (Szczesniak et al., 2016) but was missed in the Phytozome V12 annotation (Goodstein et al.,

93   2012; Lang et al., 2018). The overexpression of this peptide resulted in larger moss plant sizes

94   and a faster growth rate, whereas the KO mutant had the opposite phenotype (Fesenko *et al.*,

95   2019). Based on the observed phenotypic effects, we renamed this peptide "FAMOSS" here.

96   The inspection of the genome region around CNT2064811 revealed that the protein-coding

97   gene *Pp3c9_20610V3* is located in close proximity to this lncRNA. To exclude the possibility
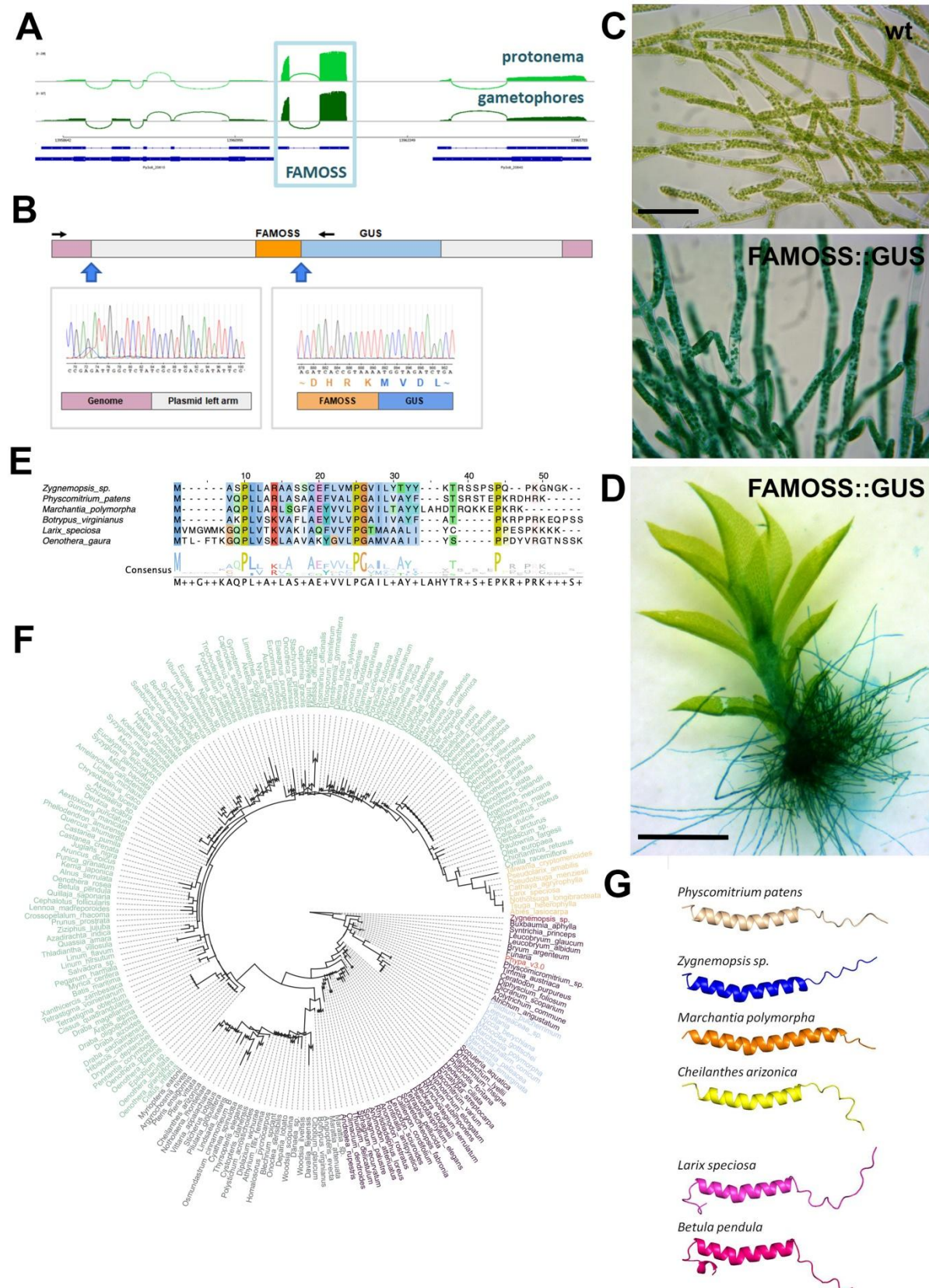
3

98   that the FAMOSS peptide is an upstream or downstream smORF located within annotated

99   mRNA, we additionally performed direct nanopore RNA sequencing (ONT DRS) on the

100   protonemal and gametophore transcriptomes (Fesenko et al., 2021). ONT DRS allows the

101   accurate assembly and identification of the exon–intron structure of the transcripts. This analysis

102   confirmed that CNT2064811 is an independent transcriptional unit with a higher transcriptional

103   level than the surrounding protein-coding genes (Figure 1A). To additionally explore whether

104   FAMOSS is translated from the predicted smORF, we used CRISPR-Cas9 to fuse a reporter

105   *GUS* sequence to the *FAMOSS* sequence in the moss genome (Figure 1B–D). We observed that

106   *FAMOSS* expression both in the protonemata and gametophores was consistent with the results

107   of the transcriptomic analysis.

108   We next analyzed the conservation of the FAMOSS peptide across different plant lineages.

109   Using a peptide amino acid sequence as a query, we performed a TBLASTN search (*E*-value

110   cutoff < 0.001) against the transcriptomes from the 1000 plants project (OneKP) and manually

111   inspected the results. This search revealed possible orthologs in the liverworts, other mosses, and

112   ferns, suggesting that this peptide was widely conserved in certain lineages (Figure 1E, F);

113   however, no hits could be detected in the hornworts, lycophytes, or vascular plants. In addition,

114   an ortholog of the FAMOSS peptide was also found in the transcriptome of *Zygnemopsis* sp.

115   (streptophyte algae). Although the C-terminal end of the FAMOSS peptide was poorly

116   conserved, the analysis of multiple alignments between the possible orthologs in green algae,

117   mosses, liverworts, and ferns revealed a pattern of highly conserved amino acid residues (Figure

118   1E). To identify potential conserved motifs in the FAMOSS peptide, the MEME algorithm

119   (Bailey et al., 2015) was used. This approach confirmed the presence of a significantly conserved

120   motif, spanning the first 30 aa of the FAMOSS peptide (Supplemental Figure 1).

121   Given that the identification of peptide homologs can be problematic in distant species, we

122   next performed a HMMER search (*E*-value cutoff < 0.01) against the translated transcriptomes

123   of selected Gymnospermae and Angiosperms species from the OneKP project (One Thousand

124   Plant Transcriptomes, 2019) and manually curated the results. This analysis revealed possible

125   orthologs in eight Gymnospermae species (12 transcripts, mean = 44 aa), 108 Core

126   Eudicots/Rosids species (124 transcripts, mean = 47 aa), 41 Core Eudicots/Asterids species (53

127   transcripts, mean = 53 aa), and 25 Basal Eudicots (38 transcripts, mean = 46 aa) (Supplemental

128   Table 1); however, further studies are needed to confirm that these peptides are true orthologs.

129   The corresponding transcripts do not encode ORFs longer than 100 aa, and 50% (63/124) of the

130   transcripts from the Core Eudicots/Rosids, 66% (35/53) from the Core Eudicots/Asterids, and

131   71% (27/38) from the Basal Eudicots were annotated as lncRNAs in a database of lncRNAs in

132   Angiosperms, AlnC (Singh et al., 2021).

4

133   According to a prediction made using TMHMM version 2.0 (Krogh et al., 2001), the *P.*
134 *patens* FAMOSS peptide contains a transmembrane domain (Fesenko et al., 2021). To further
135 investigate the relationship between the conserved amino acid residues and the structural
136 properties of FAMOSS, we predicted the *P. patens* FAMOSS 3D structure using a recently
137 developed machine learning algorithm, AlphaFold2 (Jumper et al., 2021), which was shown to
138 have promising results. According to the obtained structural model, the N-terminal and central
139 parts of the peptide represent an alpha-helix with a slight kink in its center, probably associated with
140 a proline residue. The C terminus was predicted to be disordered (Figure 1G). To further explore
141 this finding, we analyzed the structures of predicted FAMOSS orthologs from five other plants
142 from different taxonomic groups (algae, liverworts, ferns, conifers, and dicots), revealing similar
143 results overall (Supplemental Figure 2). Our findings suggest that an ortholog of the FAMOSS
144 peptide was present in the last common ancestor of land plants and streptophyte algae and widely
145 conserved in different land plant lineages. The high expression level of the corresponding
146 transcript suggests that this peptide is an unannotated highly conserved small protein.
147

148

149   **Figure 1.** FAMOSS is a widely conserved plant smORF-encoded peptide.

150   A - Sashimi plot showing *FAMOSS* transcription as confirmed using nanopore RNA

151   sequencing in *Physcomitrium patens* protonema and gametophores. B - Construction of

152   FAMOSS coupled with a GUS reporter protein at the FAMOSS promoter. Black arrows indicate

6

153 primers used for identification. C, D - GUS staining of the protonema (C, scale bar = 200 μm)
154 and gametophores (D, scale bar = 1 mm). E - The alignment of the FAMOSS peptide and
155 orthologous sequences from different plants. F - Phylogenomic tree of the identified FAMOSS
156 orthologs. Mosses, burgundy; liverworts, blue; algae, red; ferns, gray; gymnosperms, orange;
157 angiosperms, green. G - *P. patens* FAMOSS structure and structures of its orthologs, predicted
158 using AlphaFold.

159

FAMOSS regulates the tip growth rate in protonemata

161 Previously, we showed that *P. patens FAMOSS* OE mutant lines displayed a rapid
162 protonemal growth phenotype, whereas the KO lines grew more slowly than the wild-type plants
163 (Fesenko *et al.*, 2019). Moss protonemata consist of two morphologically distinguishable cell
164 types, chloronemata and caulonemata (Figure 2A). Chloronemata are produced first, as the
165 spores germinate, while caulonemal cells develop several days later at the tips of the
166 protonemata (Vidali and Bezanilla, 2012). Caulonemal cells are characterized by their higher
167 growth rate than chloronemal cells and tangential cell walls (Jang and Dolan, 2011).

168 To test the hypothesis that the rapid growth of the *FAMOSS* OE lines is due to the
169 accumulation of caulonemal filaments, the proportion of chloronemal to caulonemal cells was
170 compared in the wild-type and mutant lines. The ratio of caulonemal to chloronemal cells was
171 significantly higher in the OE line and lower in the KO line when compared with the wild type
172 (Figure 2A; $n = 3$ independent biological repeats; chi-square test, $P < 10^{-15}$). The chloronemal
173 cells therefore predominate in the KO line (Supplemental Figure 3), suggesting a link between
174 *FAMOSS* expression and the transition from chloronemal to caulonemal cells in *P. patens*. We
175 next compared the length of the apical and two subapical cells between the wild-type and mutant
176 lines. Although the lengths of the apical cells were similar in all genotypes, the subapical cells
177 were significantly longer in the OE line than in the wild type or the KO line (Figure 2B,
178 ANOVA with post-hoc Tukey HSD (Honestly Significant Difference) $P < 0.00001$). These
179 observations led to the hypothesis that the observed changes in the moss growth rate come from
180 an altered protonemal structure (caulonemata/chloronemata ratio) and increased subapical cell
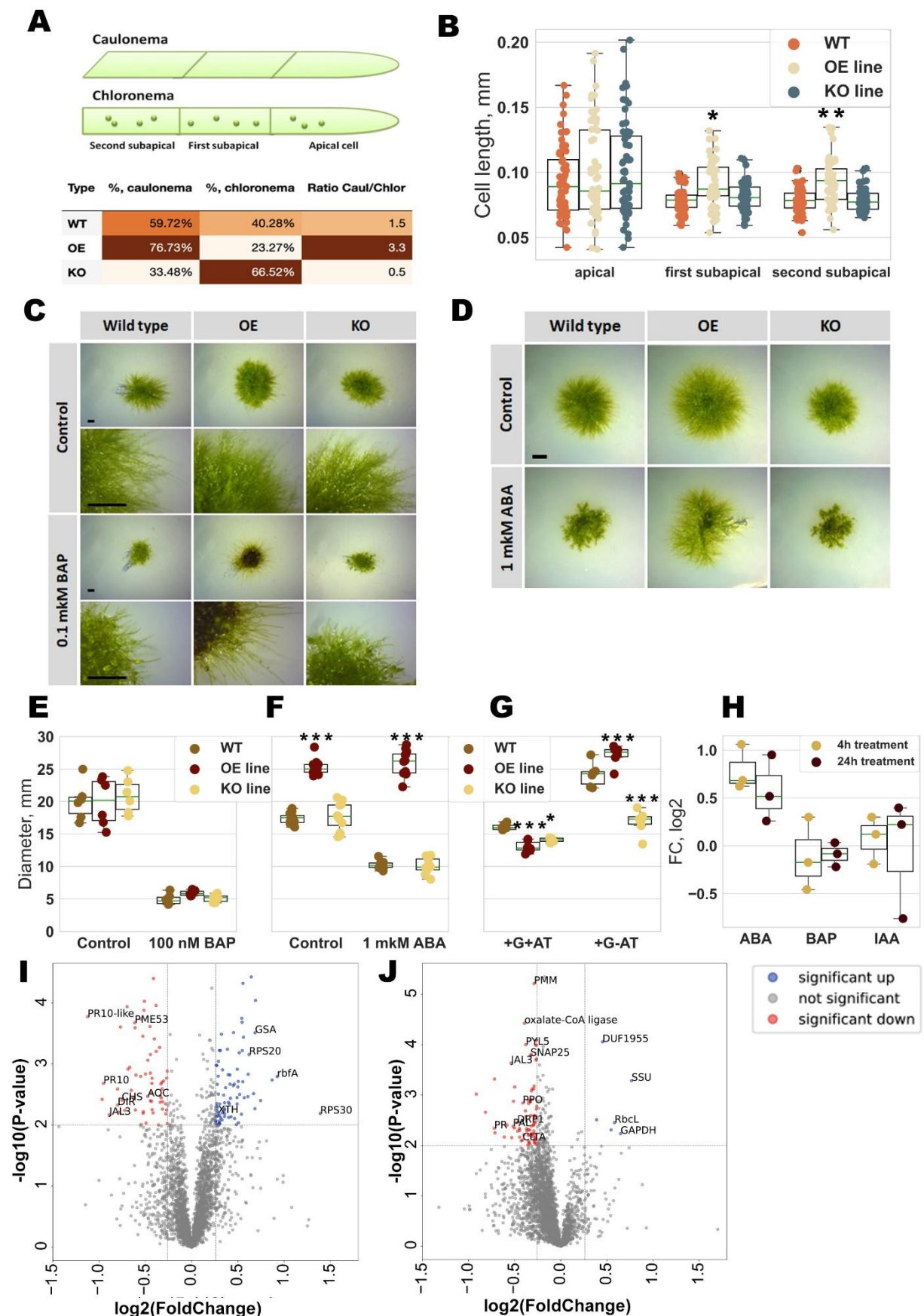181 lengths.

182 The chloronemal-to-caulonemal transition is regulated by both hormonal crosstalk and
183 different factors, such as glucose, light, and low nutrient availability (Jaeger and Moody, 2021).
184 Low light, cytokinins, and abscisic acid (ABA) are negative regulators of caulonemal

7

185   differentiation, whereas auxin, glucose, and a high light intensity are positive regulators. We

186   therefore investigated how both negative and positive regulators influence the caulonemal

187   transition in the wild-type and mutant lines (Fig. 2C–F).

188   First, we tested the influence of cytokinin and ABA treatments on the growth rate of both

189   mutant lines (Figure 2C, D). It has previously been shown that large concentrations of cytokinins

190   in the growth medium inhibit filament growth and induce callus-like structures (Sabovljevic et

191   al., 2014). In our experiments, filament growth in the wild-type and KO plants was strongly

192   inhibited under a 0.1 µM 6-benzylaminopurine (BAP) treatment, but the *FAMOSS* OE mutant

193   line produced long protonemal filaments, suggesting a decreased sensitivity to cytokinins (Figure

194   2C, E). Another negative regulator, ABA, significantly inhibited the growth of both the wild-

195   type and KO moss (Figure 2D and F; ANOVA with post-hoc Tukey HSD $P < 0.001$), but there

196   was no effect on the growth rate of the OE line. Thus, the overexpression of *FAMOSS* led to a

197   reduced sensitivity to the negative regulators of moss protonemal growth, cytokinin, and ABA.

198   Ammonium tartrate (AT) is known to reduce the transition into caulonemal cells and

199   promote chloronemal branching (Vidali and Bezanilla, 2012). Given the altered ratios of

200   chloronemal to caulonemal filaments in the mutant lines, we compared the growth of the

201   different genotypes on culture mediums with and without AT. The application of AT

202   significantly reduced the growth rates of both the wild-type and mutant plants ($P < 0.01$; Figure

203   2G), although both mutant lines significantly differed from the wild type, with the OE plants

204   being the smallest. On the medium without AT, the OE plants showed the fastest growth, but the

205   KO plants grew more slowly than the other genotypes (Figure 2G).

Figure 2. The growth of mutant lines in different conditions.

A - The ratios of the two types of moss protonema filaments, caulonemata and chloronemata, in wild-type, *FAMOSS*-overexpressing (OE), and knockout (KO) plants. B - The

9

210   lengths of the apical, first subapical, and second subapical cells. C - The effect of 6-
211   benzylaminopurine (BAP) on protonemal morphology. Scale bar = 1 mm. D − The effect of
212   abscisic acid (ABA) on protonemal morphology. E - The effect of BAP on the protonemal
213   growth rate. F - The effect of ABA on protonemal growth. G - The effect of medium
214   composition on protonemal growth. +G+AT, BCD medium supplemented with glucose and
215   ammonium tartrate; +G−AT, BCD medium with glucose but without ammonium tartrate. H −
216   Fold change (FC) in *FAMOSS* transcription after treatments with ABA, BAP, and indole-3-acetic
217   acid (IAA). I, J - Quantitative proteomic analysis of the *FAMOSS*-overexpressing (OE) and
218   knockout (KO) plants. Volcano plots of the entire set of proteins quantified in the iTRAQ
219   analysis in the *FAMOSS* OE (I) and KO (J) lines. Proteins with significant differences in
220   abundance relative to the wild type are depicted in color. GSA, glutamate-1-semialdehyde 2,1-
221   aminomutase; rbfA, ribosome-binding factor A; RPS20, ribosomal protein S20; RPS30,
222   ribosomal protein S30; AOC, allene oxide cyclase; GST, glutathione *S*-transferase; CHS,
223   chalcone synthase; XTH, xyloglucan endotransglucosylase/hydrolase protein 23; PME, pectin
224   methylesterase; rbcL, ribulose-1,5-bisphosphate carboxylase/oxygenase large subunit; GAPDH,
225   glyceraldehyde-3-phosphate dehydrogenase A chloroplastic-like isoform X2; JAL3, jacalin-
226   related lectin 3; PPO, polyphenol oxidase; PAL, phenylalanine ammonia-lyase; PR10,
227   pathogenesis-related protein; PR10-like, pathogenesis-related protein-like; DIR, dirigent protein;
228   SNAP25, synaptosomal-associated protein 25; ASPL, tether containing UBX domain for
229   GLUT4; DRP1, dynamin-related protein 1E; CLTA, clathrin light chain; PYL5, pyrobactin
230   resistance 1-like 5; PMM, phosphomannomutase; SSU, ribulose-1,5-bisphosphate
231   carboxylase/oxygenase small subunits; DUF1955, domain of unknown function.

232   *, $P < 0.05$; **, $P < 0.01$; ***, $P < 0.001$.

233

234   The stimulatory effect of auxin on the transition from chloronemal to caulonemal filaments
235   has been shown previously; however, exogenous auxin treatments resulted in the inhibition of
236   moss growth (Thelander et al., 2018). In our experiments, the growth of wild-type moss plants
237   was significantly inhibited under auxin treatment starting with 1 nM indole-3-acetic acid (IAA;
238   Supplemental Figure 4). In contrast, the growth rate of the OE line was significantly decreased
239   only by 1 μM IAA (ANOVA with post-hoc Tukey HSD $P < 0.001$). As the auxin concentration
240   increased, the protonemal filaments were increasingly composed of caulonemata, resulting in a
241   sparser and lighter appearance. Thus, *FAMOSS* is expressed in conditions favorable to
242   caulonemata formation, causing chloronemata to differentiate into caulonemata, which increases
243   the protonemal growth rate.

10

244   We next tested whether the auxin and cytokinin treatments influenced the transcriptional
245   level of *FAMOSS*; however, no difference was observed after a 4- or 24-h treatment with either
246   phytohormone (Figure 2H). By contrast, *FAMOSS* expression was marginally upregulated by
247   ABA (two-tailed t-test, $P < 0.05$). Our findings showed that the overexpression of *FAMOSS*
248   positively regulates protonemal growth and the transition from chloronemal to caulonemal
249   filaments. In particular, sensitivity to the hormonal negative regulators of the caulonemal
250   transition was reduced in the OE line. In addition, the proportion of caulonemal filaments was
251   reduced in the KO plants, which had a similar phenotype to the wild-type plants, although the
252   growth rate was lower on the medium without the inhibitor of caulonemal growth (AT).

Proteomic analysis of the mutant lines

254   We next used isobaric tags for relative and absolute quantitation (iTRAQ)-based
255   comparative quantitative proteomic analyses to identify changes in the proteomes of the mutant
256   lines. Because iTRAQ quantification underestimates the amount of real fold change (Ow et al.,
257   2009), fold change ratios of >1.20 or <0.83 ($P < 0.01$, one-way ANOVA) were used to identify
258   differentially expressed protein groups (DEPs). Overall, we identified 118 DEPs in the OE line
259   and 75 DEPs in the KO line (Figure 2I, J; Supplemental Table 2).

260   The most upregulated DEPs in the OE line were ribosomal proteins, such as Pp3c2_29010
261   (RP-S30e), Pp3c24_17080 (RP-S20), and Pp3c12_16410 (rbfA) (Figure 2I). Among the most
262   downregulated DEPs in the OE line, we identified a group of proteins that participate in the
263   stress response; for example, the pathogenesis-related proteins (PR-10) Pp3c2_27350 and
264   Pp3c7_19850 were previously shown to be involved in the defense response (Castro et al., 2016)
265   and downregulated under osmotic stress (Stevenson et al., 2016). In addition, proteins related to
266   the biotic stress response were downregulated, including Pp3c5_22560 (dirigent protein; DIR),
267   Pp3c5_22560 (chalcone synthase; CHS), and Pp3c4_22490 (allene oxide cyclase; AOC). Stress-
268   induced DIR plays a role in the adaptive response (Paniagua et al., 2017), while CHS is a key
269   enzyme of the flavonoid/isoflavonoid biosynthesis pathway and is involved in the salicylic acid
270   biosynthesis pathway (Dao et al., 2011). AOC is involved in the jasmonic acid biosynthesis
271   pathway (Stenzel et al., 2003). Another protein related to secondary metabolism regulation and
272   the defense response is Pp3c9_1620 (polyphenol oxidase; PPO) (Tran et al., 2012). The protein
273   pectin methylesterase (Pp3c5_12660) was also downregulated in the OE line. Pectin
274   methylesterases modulate the cell wall mechanical properties and organ initiation in Arabidopsis
275   (Peaucelle et al., 2011). These findings therefore suggest that the OE line would be less resistant

11

276   to a variety of stress conditions. However, additional experiments are needed to confirm or

277   dismiss this hypothesis.

278   The proteome changes in the KO line were less pronounced (Figure 2J). The chloroplastic

279   proteins, such as the large and small subunits of RuBisCO and Pp3c11_15790 (glyceraldehyde

280   3-phosphate dehydrogenase (GAPDH)), were among the most upregulated in the KO line

281   (Supplemental Table 2). One possible explanation for this result is the predominance of

282   chloroplast-rich chloronemal filaments in this line. The stress-related proteins were also

283   downregulated in the KO line, as was seen in the proteome of the OE line; for example,

284   Pp3c7_19850 (PR10), Pp3c6_6545 (DIR-related), and Pp3c1_18940 (phenylalanine ammonia-

285   lyase; PAL) were downregulated. It is worth noting that Pp3c7_19850 (PR10), Pp3c18_10760

286   (glutamine synthetase), Pp3c9_1620 (polyphenol oxidase), and Pp3c1_1940 (jacalin-like lectin

287   domain) were downregulated in both the OE and the KO lines. The top 10 most downregulated

288   proteins included two proteins containing the cupin (Cupin_2) domain (Supplemental Table 2).

289   Proteins with this domain play crucial roles in plant development and defense (Wang et al.,

290   2014).

291   We also identified a group of downregulated DEPs associated with vesicle trafficking in

292   the KO line. These were dynamin-related protein 1C (DRP1C, Pp3c19_4870), which regulates

293   vesicle formation in post-Golgi trafficking (Fujimoto and Tsutsumi, 2014; Jilly et al., 2018);

294   clathrin light chain (Pp3c7_10220; CTLA); and synaptosomal-associated protein-related

295   (Pp3c2_7850; SNAP25). SNAP25 is a SNARE (soluble N-ethylmaleimide-sensitive factor

296   attachment protein receptor) protein, which is involved not only in vesicular trafficking under

297   normal conditions but also in regulating transport of cell wall–associated and defense proteins

298   during biotic stress (Kwon et al., 2020). SNARE-mediated membrane trafficking is also required

299   for the proper response of plants to abiotic stresses.

300   The iTRAQ analysis thus showed that proteins involved in the response to different stress

301   conditions were downregulated in both mutant lines. By contrast, the most upregulated DEPs in

302   the OE line belong to biosynthetic processes, suggesting that the rapid growth rate in the OE line

303   is linked to proteome changes.

304   **The stress response is altered in the mutant lines**

305   According to the quantitative proteomic analysis, some stress-related proteins were

306   downregulated in both mutant lines, suggesting that they may have altered stress tolerances. In

307   addition, the reduced sensitivity to ABA observed in the OE line could decrease its resistance to

308   abiotic stress factors.
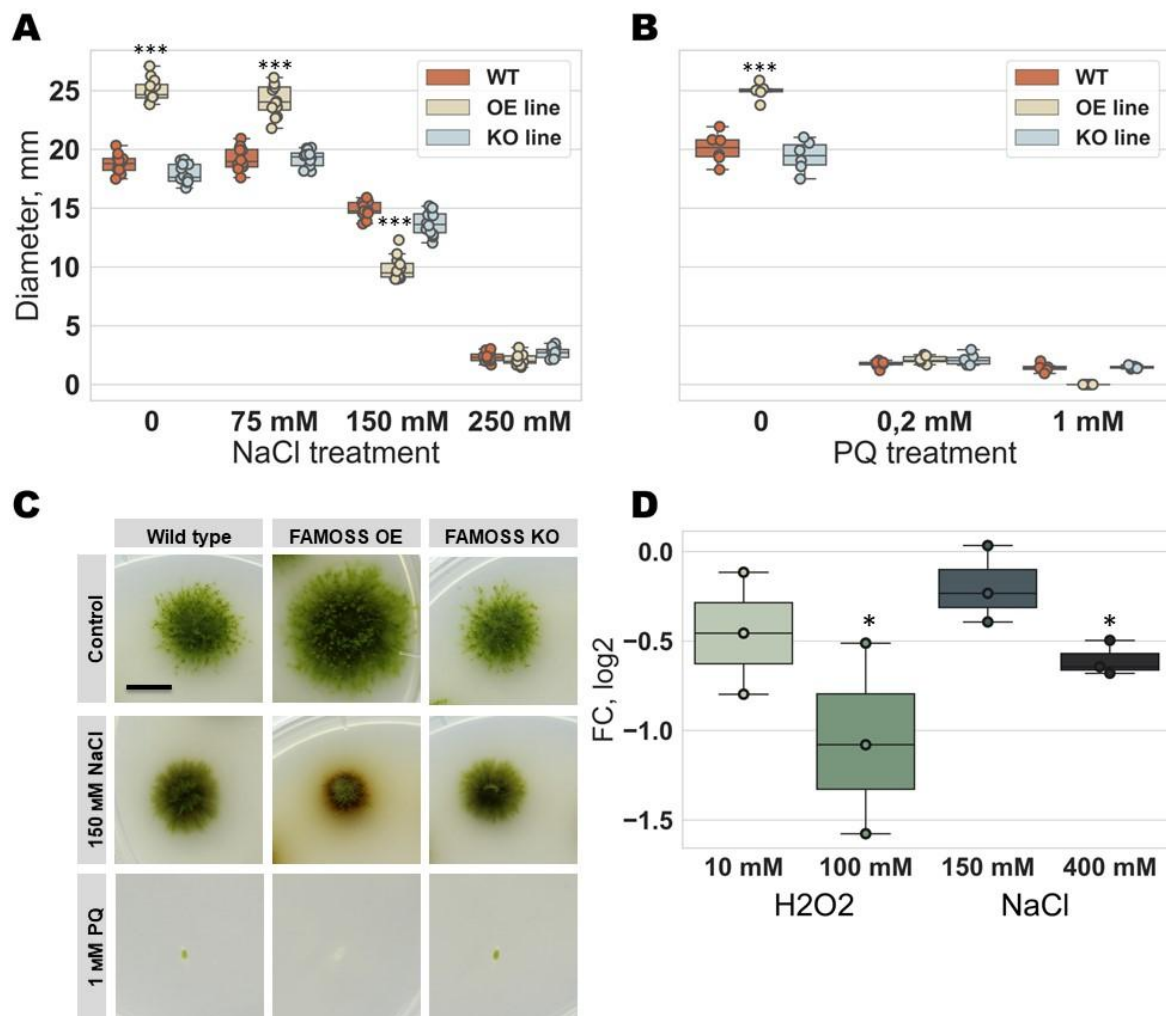
309
310 **Figure 3.** The growth rate of the mutant lines under stress-related conditions

311 A - Effect of NaCl on protonemal growth. B - Effect of paraquat (PQ) on protonemal growth. C -
312 Effect of NaCl and PQ on protonemal morphology after 30 days of cultivation. D - *FAMOSS*
313 expression under different stresses. *, $P < 0.05$; ***, $P < 0.001$.

314   We next investigated the growth of both the mutant and wild-type plants under abiotic
315 stress conditions induced by salt (NaCl) and paraquat (PQ) (Figure 3A-C). All genotypes were
316 severely affected starting with the 150 mM NaCl concentration (Figure 3A); however, the
317 growth rate of the OE plants was significantly reduced compared with the wild type and KO
318 under this concentration of NaCl ($P < 0.001$, ANOVA with post-hoc Tukey HSD test).
319 Moreover, the OE line had the most severely altered phenotype after the 150 mM NaCl treatment
320 (Figure 3C).

321   PQ is a potent reactive oxygen species (ROS) inducer. The growth of all genotypes was
322 significantly inhibited by a treatment with either 0.2 or 1 mM PQ ($P < 0.001$, ANOVA with

13

323   post-hoc Tukey HSD test; Figure 3B, C). Moreover, the growth of the OE line was completely

324   inhibited and the plants died under 1 mM PQ (Figure 3C).

325   Using RT-qPCR analysis, we found that the level of *FAMOSS* transcription in the wild-

326   type protonemata was only marginally decreased after a 1-h treatment with 400 mM NaCl or 100

327   mM H_2O_2 (two-tailed t-test, $P < 0.05$; Figure 3D). This result suggests that *FAMOSS* is not

328   stress-inducible at the transcriptional level.

329   Our results showed that the mutants, especially the OE line, had a reduced ability to adapt

330   to stress. Given that ABA is the most important regulator of the abiotic stress response, the rapid

331   protonemal growth and altered ABA sensitivity in the *FAMOSS* OE line could result in the

332   observed phenotypes.

FAMOSS interactome

333

334   We further investigated the possible protein interaction partners of the FAMOSS peptide

335   using two approaches, a pull-down assay and coimmunoprecipitation (co-IP) (Figure 4A-C). For

336   the pull-down assay, a recombinant FAMOSS peptide fused with streptavidin at the N-terminal

337   end (FAMOSS-SAV; see Materials and Methods) and recombinant streptavidin were used

338   (Figure 4B). We used reversible cross-linking to bind the interacting proteins and identified them

339   using a mass spectrometry (MS) analysis. This approach revealed 323 unique protein groups in

340   the FAMOSS-SAV samples (Supplemental Table 3). Besides the large clusters of ribosomal and

341   chloroplast proteins, which are common contaminants (Mellacheruvu et al., 2013), the most

342   promising protein partners were Rab-type small GTPases (Figure 4D). Rab proteins participate

343   in a diverse range of cellular processes, including vesicular trafficking, tip growth, and the stress

344   response (Chen, Heo, 2018; Lycett, 2008; Ma, 2007). Because many contaminants were

345   observed in the FAMOSS-SAV interactomes, we performed a gel electrophoresis analysis of the

346   samples and analyzed the 25-kDa band using an in-gel trypsin digestion followed by a liquid

347   chromatography (LC)–MS/MS analysis to enrich the fraction of Rab proteins.

348   The final list of Rab-type GTPases, unique for FAMOSS-SAV samples, included

349   RabD2B/Rab-1A, RabA2B/Rab-11A, RabF/Rab-5, RabA5A/Rab-11A, RabE/Rab-8A, and

350   RabG/Rab-7A (Figure 4D; Supplemental Table 3). Among these proteins, the largest peptides

351   coverage (33%) and intensity were observed for the Pp3c14_15250 (RabA2B/Rab-11A) protein.

352   To validate the obtained results, we generated mutant lines overexpressing FAMOSS-

353   FLAG fusion constructs (Figure 4A). The FLAG tag was placed on the C terminus (mutant 1028

354   line) or on the N terminus (mutant 1032 line) of the FAMOSS peptide (Figure 4B). We

14

355 immunoprecipitated FLAG-tagged FAMOSS and identified RabD2B/Rab-1A, RabA2B/Rab-
356 11A, RabA5A/Rab-11A, and RabE/Rab-8A in the interactome of the 1032 line (*n* = 3
357 independent experiments) (Figure 4D). These proteins were unique for the FAMOSS-FLAG
358 interactomes and were not found in the control samples.

359 Due to high sequence similarity of Rab GTPases (Figure 4E; Lycett, 2008; Ma, 2007;
360 Minamino and Ueda, 2019), we cannot rule out the possibility that FAMOSS peptide interacts
361 with several Rab proteins. For example, human GDI1 protein was shown to interact with
362 different Rab GTPases: RAB3A, RAB5A, RAB5B, RAB5C, RAB8A, RAB8B, RAB10, RAB35
363 and RAB43 (Steger et al., 2017). In addition, due to similar subcellular localization (Elliott et al.,
364 2020) Rab proteins from different families could co-purify together in our experiments.

365 Thus, our results suggest that the Rab GTPase proteins may interact with the FAMOSS
366 peptide. The Rab GTPase proteins target vesicles to the plasma membranes and mediate their
367 fusion, thereby stimulating the intensity of vesicular trafficking to the cell apex and increasing
368 the tip growth rate (Lycett, 2008; Ma, 2007). This is consistent with the phenotype of the
369 *FAMOSS* OE lines.

370

371

15
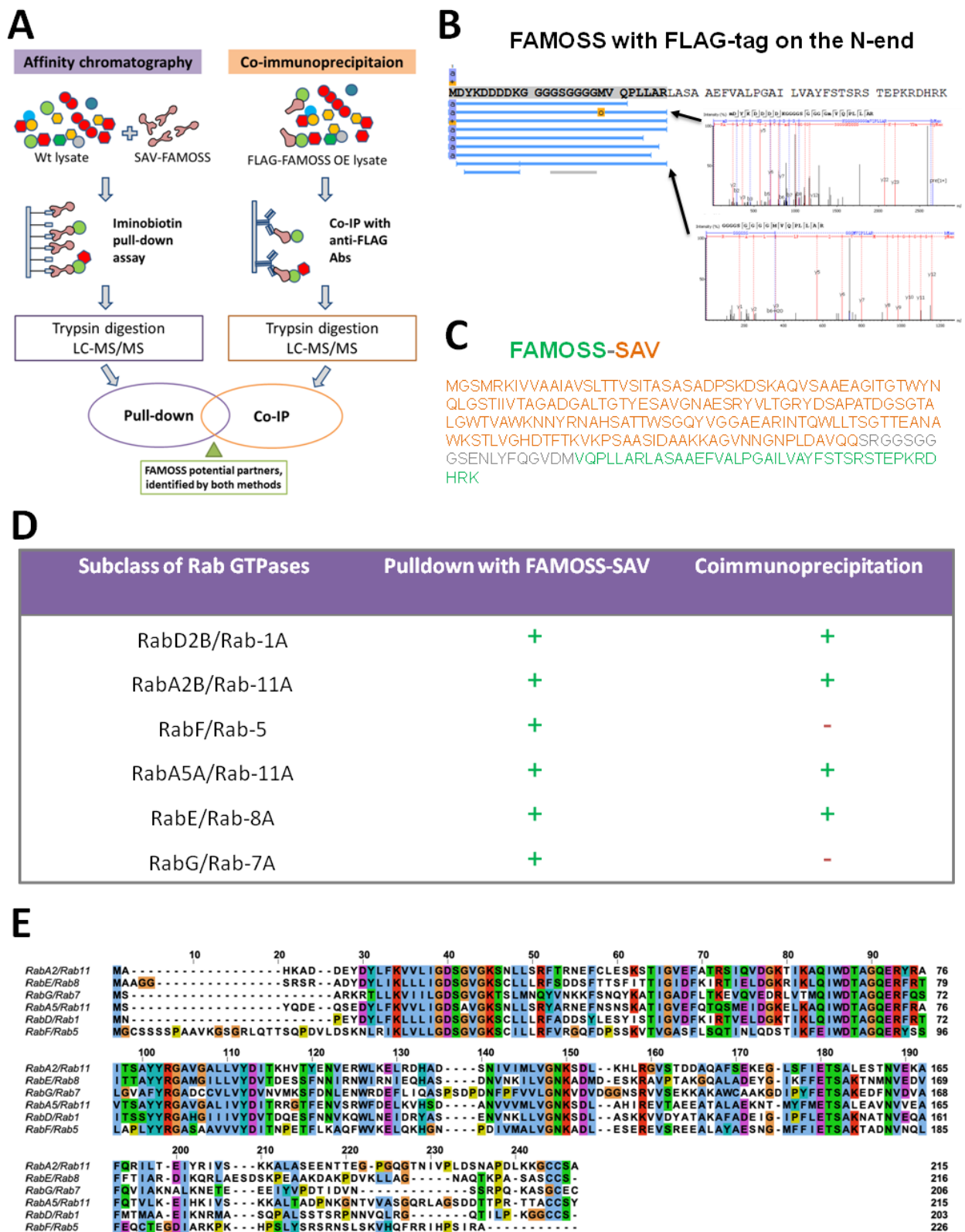
Figure 4. Analysis of the protein partners of the FAMOSS peptide. A - Diagram of the interactome experiments. B - Sequence and coverage of the FLAG-tagged FAMOSS sequence. C - Sequence of streptavidin (SAV)-tagged FAMOSS. D - Rab GTPases present in the two types of interactome experiments. Proteins detected in samples are marked with a plus sign, and those

377 not detected are indicated with a minus sign. E – Alignment of Rab GTPases found in the
378 FAMOSS interactomes.

379

FAMOSS regulates vesicular trafficking

381 The moss protonemal filaments expand by polarized tip cell growth similar to pollen tubes
382 or root hairs in flowering plants (Orr et al., 2020; Rensing et al., 2020; Rounds and Bezanilla,
383 2013; Vidali and Bezanilla, 2012). It is well known that plant tip growth requires active apical
384 vesicular trafficking regulated by different families of small GTPases, including Rab proteins
385 (Minamino and Ueda, 2019). The RabA GTPases were previously shown to regulate polarized
386 secretion and vesicle delivery in plants (Chen, Heo, 2018; de Graaf et al., 2005; MartiniEre and
387 Moreau, 2020; Szumlanski and Nielsen, 2009).

388 To determine whether the FAMOSS peptide influences the vesicle pool in the apex cells,
389 we labelled protonemal filaments of the wild type and both mutant lines using the fluorescent
390 dye SynaptoGreen C4 (also known as FM1-43, a trademark of Molecular Probes) (Jelinkova et
391 al., 2010) (Figure 5A–C). The FM1-43 dye is widely used for a marking of vesicles in the tip
392 growing plant cells such as pollen tube, root hair and protonema apical cells (Samaj et al., 2005;
393 Bove et al., 2008; Pleskot et al., 2012; Gisbergen et al., 2020). In the wild-type cells, the
394 distribution of the apical vesicles was similar to that which was previously described in *P. patens*
395 (Rawat et al., 2017; Gisbergen et al., 2020) (Figure 5B); however, the labelling intensity was
396 significantly increased in the OE line compared with both the wild-type and KO lines (ANOVA,
397 $P < 0.001$; Figure 5D, E). This suggests a more intensive vesicle trafficking in the cell apex,
398 which is consistent with the rapid protonemal growth in the OE line. By contrast, the
399 fluorescence intensity was significantly decreased in the cell apexes of the protonemal filaments
400 in the KO line compared with the wild-type and OE line cells (ANOVA, $P < 0.001$; Figure 5E).

401 These results suggest that the FAMOSS peptide may function as a possible modulator of
402 vesicular trafficking during tip cell growth via its interaction with the Rab small GTPases.

403

17
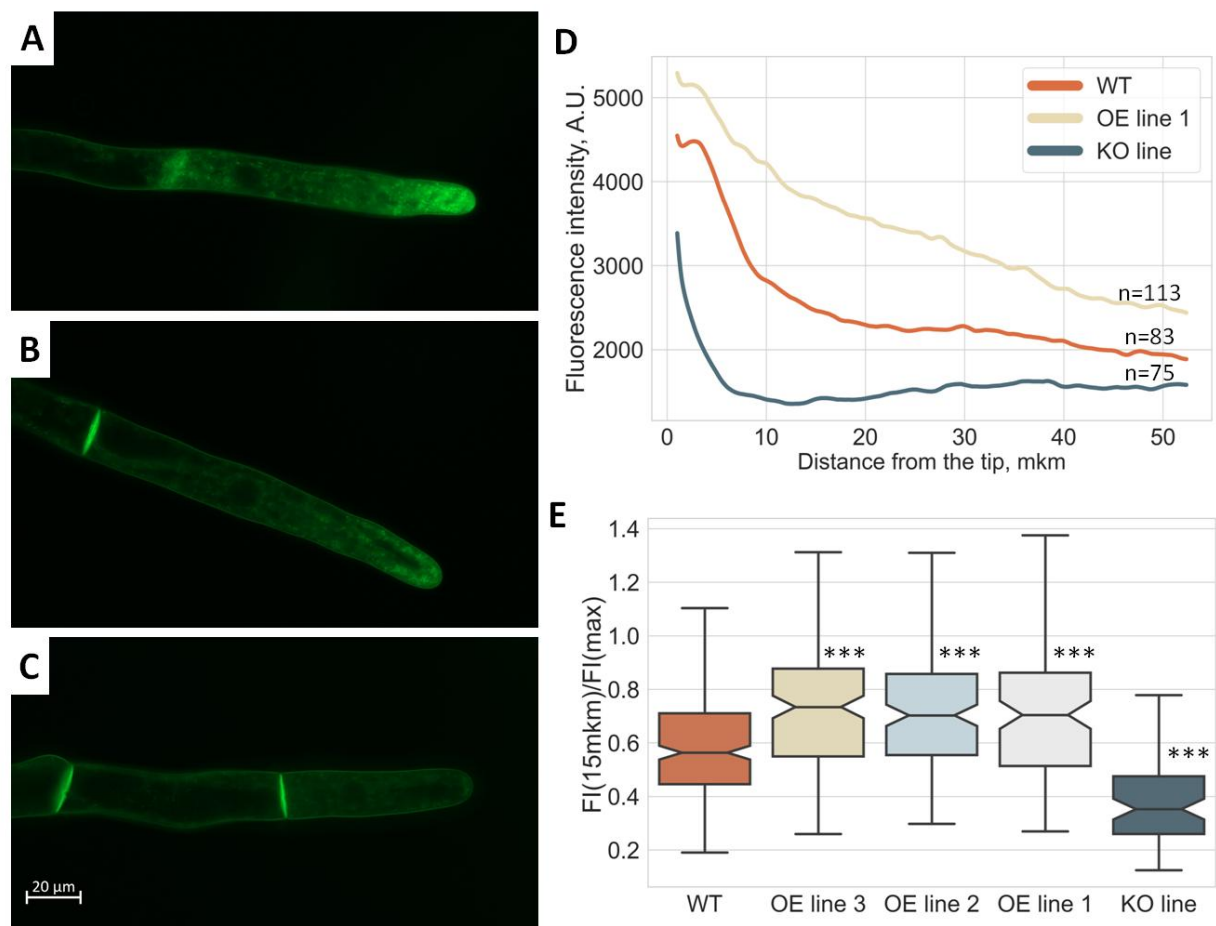
Figure 5. The FAMOSS peptide affects vesicular trafficking. A–C - Apical protonemal cells stained with SynaptoGreen C4. (A – *FAMOSS*-overexpression line (OE); B – The wild type; C - *FAMOSS* knockout line (KO). D - Profile of SynaptoGreen C4 fluorescence in the apical cells. E - Boxplot showing the ratios of intensity of SynaptoGreen C4 staining at the distance 15 mkm from the cell tip to the maximal intensity. ***, $P < 0.001$.

Given that apical vesicular transport is linked to cell wall formation (Rounds and Bezanilla, 2013), we next analyzed the regeneration of the protonemal filaments after protoplast isolation. The proportion of regenerated plants with new chloronemal filaments was significantly higher in the KO line (~18%) than in the wild type (~8%) or the OE line (~2%; chi-squared test $P < 10^{-10}$). The FAMOSS peptide therefore appears to inhibit the process of chloronemal formation, which results in a more effective regeneration process in the KO line. This correlates with the observed chloronemata/caulonemata ratio in the protonemal tissue.

18

Discussion

420

421   A growing body of evidence suggests that the peptides or microproteins encoded by
422 smORFs may play important roles in animal and plant cells (Casson *et al.*, 2002; Huang *et al.*,
423 2017; Matsumoto *et al.*, 2017; Polycarpou-Schwarz *et al.*, 2018; Rohrig *et al.*, 2002; Slavoff *et*
424 *al.*, 2014; Tavormina et al., 2015); however, there are few examples of functional SEPs in plants.
425 In our previous study, we identified a new 41-aa sORF-encoded peptide that influences moss
426 growth located on a transcript predicted to be a lncRNA (Fesenko *et al.*, 2019).

427   In this study, we identified possible FAMOSS orthologs in liverworts, mosses, ferns,
428 conifers, and eudicots, indicating that it is widely conserved across the plant kingdom. A
429 FAMOSS ortholog was also found in *Zygnemopsis* sp. (streptophyte algae). This is consistent
430 with the findings that the Zygnematophyceae appear to be the closest relatives of land plants
431 (Delwiche and Cooper, 2015; Nishiyama et al., 2018; One Thousand Plant Transcriptomes,
432 2019). The corresponding transcripts do not encode longer (>100 aa) proteins, suggesting that
433 the *FAMOSS* orthologs can be considered the main ORFs. The conservation of the *FAMOSS*
434 peptide across different plant lineages is consistent with our results, in which a set of Rab-type
435 small GTPases were identified in the FAMOSS interactomes (Table 1). Rab GTPases are highly
436 conserved regulators of membrane trafficking in plants (Lycett, 2008; Ma, 2007; Minamino and
437 Ueda, 2019) and are present in both algae (Hoepflinger et al., 2013) and land plants (Minamino
438 and Ueda, 2019). In particular, proteins from the RabA clade are involved in the coordination of
439 tip cell growth (Ma, 2007); for example, these proteins are crucial for the tip-targeted vesicular
440 trafficking of cell wall components in root hairs (Preuss et al., 2004) and pollen tubes
441 (Szumlanski and Nielsen, 2009) in Arabidopsis. Tip growth of the moss protonemata is also
442 regulated by the Rab proteins (Orr et al., 2021); thus, the consideration of Rab GTPases as
443 possible partners of the FAMOSS peptide is consistent with the protonemal growth rates,
444 subapical cell lengths, and chloronemata-to-caulonemata transition in the mutant lines.
445 Moreover, using the fluorescent dye SynaptoGreen C4, we revealed changes in the intensity of
446 the vesicular trafficking in the mutant lines. A previous study showed that the AtRabA1d protein
447 accumulated in the apical dome of the growing root hairs in Arabidopsis, completely
448 colocalizing with intracellular vesicles stained with the fluorescent dye FM4-64 (Ovecka et al.,
449 2010). In addition, the quantitative proteomic analysis revealed that some proteins associated
450 with vesicular trafficking were downregulated in the KO plants. Considering results from
451 different experiments, we hypothesize that the interaction of the FAMOSS peptide with Rab

19

452 GTPases or with proteins from the corresponding protein complex may affect the intensity of
453 vesicular trafficking in the moss tip cells and influence the protonemal growth rate.

454   In addition to regulation of tip growth in plants, Rab proteins are also involved in
455 phytohormone signaling and the stress response. AtRabE1c interacts with the ABA receptor
456 PYL4 (pyrobactin resistance 1-like 5) to stimulate the ABA response and stress tolerance in
457 Arabidopsis (Chen et al., 2021), while the overexpression of *OsRab11* in rice (*Oryza sativa*)
458 resulted in a decreased plant sensitivity to ABA and enhanced plant tolerance to salt and osmotic
459 stresses (Chen, Heo, 2018). Here, we found that *FAMOSS* OE plants were less sensitive to ABA
460 treatment and strongly inhibited by salt stress. Moreover, the stress-related proteins were
461 downregulated in both the *FAMOSS* OE and KO lines, suggesting a link between the functions
462 of the Rab proteins and *FAMOSS* expression levels.

463   In conclusion, we described the functions of a new plant SEP encoded by a lncRNA in the
464 moss *P. patens*. We suggest that this peptide, named FAMOSS, is a possible interaction partner
465 of the Rab GTPases, which in turn control numerous processes, including vesicular trafficking,
466 polar tip growth, phytohormone signaling, and stress tolerance, processes that were altered in the
467 *FAMOSS* OE/KO mutants. The *FAMOSS* peptide could therefore be considered an important
468 component of Rab signaling in plants. Further studies will help elucidate the mechanisms of such
469 interactions.

Acknowledgments

Author contributions

474 A.M. and I.F. conceived and designed experiments. A.M. and I.F. wrote the manuscript with
475 input from all authors. I.F. supervised the project. A.K and A.G. performed nanopore sequencing
476 and analyzed the sequencing data. A.M., S.K. and R.Z. performed the proteomics analysis. A.M.,
477 N.G., I.S., V.R., A.N. and A.F. conducted analysis of phenotypes and fluorescent microscopy.
478 N.G. and A.K. analyzed transcription using RT-PCR. I.F. performed the statistical and
479 bioinformatics analyses. A.K., D.K., V.M. and V.L. created genetic construction, generate
480 recombinant proteins, and performed moss transformation experiments. I.S., M.P. and A.M.
481 performed pull-down and co-immunoprecipitation. All authors read and approved the final
482 manuscript.

20

483 ## Declaration of Interests

484 The authors declare no competing interests.

485 # Materials and Methods

486 ## Physcomitrium patens growth conditions

487 *Physcomitrium patens* subsp. patens ("Gransden 2004", Frieburg) protonemata of wild
488 type and FAMOSS (PSEP1) - knockouting and overexpressing lines (Fesenko *et al.*, 2019) were
489 grown on BCD medium supplemented with 5 mM ammonium tartrate (BCDAT) and/or 0.5%
490 glucose during a 16-h photoperiod at 25 C in 9-cm Petri dishes (Nishiyama et al. 2000). Growth
491 rate measurements were taken at 30 day. The images of protonemal tissues and cells were
492 obtained by a Microscope Digital Eyepiece DCM-510 attached to a Stemi 305 stereomicroscope
493 (Zeiss, Germany) or Olympus CKX41 (Olympus, Japan) at 10 or 30 day. Seven-day-old
494 protonema tissues grown in liquid BCDAT medium were used for proteomic, pull-down assay,
495 co-immunoprecipitation and qRT-PCR analyses. The gametophores were grown on free-
496 ammonium tartrate BCD medium under the same conditions, and 8-week-old gametophores
497 were used for the further analysis.

498 ## Quantitative reverse transcription real-time PCR

499 Total RNA from protonema and gametophores was isolated as previously described (Cove
500 et al., 2009). RNA quality and quantity were evaluated via electrophoresis in an agarose gel with
501 ethidium bromide staining. The concentration of total RNA was measured using a Quant-iT™
502 RNA Assay Kit (Thermo Fisher Scientific), 5–100 ng on a Qubit 3.0 (Invitrogen, US)
503 fluorometer. The cDNA for qRT-PCR was synthesized using an MMLV RT Kit (Evrogen,
504 Russia) according to the manufacturer's recommendations employing oligo(dT)17 -primers from
505 2 µg total RNA after DNase treatment. The primers were designed using Primer-BLAST (Ye et
506 al., 2012) (Supplemental Table 4).

507 ## Confirmation of *FAMOSS* transcription using nanopore RNA

508 Nanopore data were downloaded from the BioProject with the accession number
509 PRJNA681088 (Fesenko et al., 2021). Reads were mapped against the genome Physcomitrium

21

510   patens V3.3 (Lang *et al.*, 2018) by minimap 2.17 (Li, 2016) with the following parameters: -ax

511   splice -uf -k14 f -G2k. ONT reads with a primary alignment to the genome were retained. The

512   obtained 'SAM' files were sorted and indexed with 'SAMtools'(Li et al., 2009). Sashimi plot

513   was constructed in IGV v2.6.3 (Thorvaldsdottir et al., 2013).

Generation of the overexpressing lines with FAMOSS-FLAG peptides

515   The FAMOSS sequences fused with FLAG (DYKDDDDK) tag were obtained by PCR

516   with genomic DNA as a template and primers listed in the Supplemental Table 4. Amplicons

517   were cloned into the pPLV27 vector (GenBank JF909480) using the ligation-independent

518   cloning (LIC) procedure (Aslanidis and de Jong, 1990; De Rybel et al., 2011). The resulting

519   plasmids - pPLV27-pep4-g4s-C-flag and pPLV27-N-flag-g4s-pep4 contain the C-terminus or the

520   N-terminus FLAG-fused FAMOSS peptides respectively (Supplemental Figure 5). Before

521   transformation, the plasmids were purified by Qiagen Plasmid Maxi Kit (Qiagen, Germany).

522   Moss protoplasts were transformed with circular pPLV27-pep4-g4s-C-flag and pPLV27-N-flag-

523   g4s-pep4 plasmids. Mutant lines with the overexpression of fused FAMOSS-FLAG peptides

524   were generated as described previously (Fesenko *et al.*, 2019)

CRISPR/Cas9-directed fusion with β-D-glucuronidase (GUS) protein

526   The β-glucuronidase (GUS) reporter gene system was used to study spatial expression of

527   FAMOSS peptide. The peptide coding sequence was used to search for CRISPR RNA (crRNA)

528   preceded by a *S. pyogenes* Cas9 PAM motif (NGG) using the web tool CRISPR DESIGN

529   (http://crispr.mit.edu/). The crRNA closest to the stop codon of FAMOSS peptide was selected

530   for cloning. The mutant lines with FAMOSS coding sequence fused with GUS reporter protein

531   were created using the CRISPR/Cas9 system and the pTZ-donor4 plasmid (Supplemental

532   Methods). Protoplasts were transformed with circular sgRNA, pTZ-donor4 and pBRF as

533   previously described (Fesenko *et al.*, 2019).

GUS activity assay

535   Histochemical GUS staining was carried out using β-Glucuronidase Reporter Gene

536   Staining Kit (Sigma-Aldrich) according to the manufacturer's recommendations. Moss tissues

537   were vacuum-infiltrated with Staining Solution for 2 minutes and incubated at 37°C overnight (>

538   16 hours). Stained samples were imaged by Microscope Digital Eyepiece DCM-510 attached to

22

539   a Stemi 305 stereomicroscope (Zeiss, Germany) or Olympus CKX41 (Olympus, Japan) in the
540   bright-field.

The conservation analysis

542   To identify the FAMOSS orthologs in different plant taxa, TBLASTN search with default
543   parameters was performed using CNGBdb BLAST Service for 1000 Plants (oneKP or 1KP)
544   trancriptomes (https://db.cngb.org/onekp/). The alignments were filtered by E-value $<10^{-3}$ cut-off
545   and manually curated.

546   The full peptide sequences from TBLASTN search were then aligned with MAFFT v. 7
547   (Katoh and Standley, 2013) and transformed into an HMM profile by hmmbuild tool from
548   HMMER v3.3.2 package (Eddy, 2011). Orfipy tool (Singh and Wurtele, 2021) was used to
549   predicted proteins (> 30 aa) from the transcriptomes of conifers and eudicots species that were
550   downloaded   from
551   https://datacommons.cyverse.org/browse/iplant/home/shared/commons_repo/curated/oneKP_cap
552   stone_2019. Hmmsearch tool (hammer.org, $E < 0.01$) was used to identify possible FAMOSS
553   orthologs in this protein dataset and obtained hits were manually curated.

Sequence Alignment and Conserved Motif Identification

555   The full amino acid sequences of the identified FAMOSS orthologs were extracted from
556   the corresponding transcripts and used for multiple alignments using MAFFT v.7 with default
557   settings. The resulting multiple sequence alignment (MSA) was inspected and adjusted
558   manually. The online programs MEME (Multiple Expectation Maximization for Motif
559   Elicitation; https://meme-suite.org/meme) with default parameter settings were used to search for
560   conserved motifs.

The phylogenetic analysis of the FAMOSS orthologs

562   We reconstructed a maximum-likelihood (ML) phylogenetic tree based on the entire MSA
563   of 250 orthologs using IQ-TREE v.1.6.12 (Nguyen et al., 2015) with autodetected models
564   (JTTDCMut+G4 model). Extremely divergent sequences were excluded from the analysis. The
565   phylogenetic trees were generated by the Toytree package (Eaton et al., 2020).

Prediction of FAMOSS 3D-structure

566

567   In order to predict FAMOSS peptide 3-D structure we used AlphaFold2 (Jumper *et al.*,
568 2021) algorithm, which was run as Google Colaboratory project on GitHub with custom multiple
569 sequence alignment (MSA) option. For MSA construction for a particular peptide we firstly
570 obtained a list of 100 mostly similar sequences using BLASTP search against a file
571 containing possible FAMOSS homologs. We then performed multiple protein alignment with M-
572 COFFEE online tool with default parameters (http://tcoffee.crg.cat/apps/tcoffee/do:mcoffee
573 (Notredame et al., 2000). Resulting MSA .fas file was used in the algorithm with default
574 parameters. Structures were visualised with PyMol v.2.3.0
575 (https://github.com/schrodinger/pymol-open-source).

LC-MS/MS analysis and protein identifications

576

577   Quantitative proteomic analysis was conducted as described previously (Spechenkova et
578 al., 2021). Additional details are described in the Supplemental Methods. Briefly, proteins were
579 extracted by phenol extraction method (Faurobert et al., 2007), digested by 1 µg sequence-grade
580 modified trypsin (Promega, Madison, WI, USA) at 37 ˚C overnight, iTRAQ labelling (Applied
581 Biosystems, Foster City, CA, USA) was conducted according to the manufacturer's
582 manual. Proteins were labelled with the iTRAQ tags as follows: Wild type − 113, 114, 115
583 isobaric tags, FAMOSS OE and KO − 116, 117, 118 ones. The samples after pull-down assay
584 and co-immunoprecipitation were also digested by 1 µg sequence-grade modified trypsin
585 (Promega, Madison, WI, USA) at 37 ˚C overnight in the same manner, but were not labeled by
586 iTRAQ labels. LC-MS/MS analysis was carried out on an Ultimate 3000 RSLCnano HPLC
587 system connected to a QExactive Plus mass spectrometer (Thermo Fisher Scientific, USA).
588 Tandem mass spectra were analysed by PEAKS Studio version 8.0 software (Bioinformatics
589 Solutions Inc., Waterloo, Canada). The custom database was built from Phytozome database *P.*
590 *patens* combined with chloroplast and mitochondrial proteins (33,053 records).

Pull-down assay

591

592   The plasmids pET-mSAV and pET-mSAV-pep4 were generated based on pET-plasmid
593 (Novagen, USA) and contained sequence coding for mature streptavidinstreptavidine (SAV)
594 fused with the sequences for TEV-proteinase site (pET-mSAV) or the same sequences fused
595 with and FAMOSS peptide (pET-mSAV-pep4). The *E. coli* Rosetta 2 (DE3) strain was used to

24

596 obtain recombinant proteins. Expression was induced by adding IPTG to a final concentration of
597 0,5 mM. The cells were disrupted by sonication using a Branson Sonifier 250 (VWR Scientific,
598 USA) sonicator according to the manufacturer's instructions. The lysate was purified by
599 centrifugation (15,000× g, 25 min) and washed twice with 1% (v/v) Triton X-100. The pellet was
600 dissolved in 6M guanidine chloride, pH 1,5, dialysed against 200 mM NaHCO3 pH 8,0 and
601 purified using iminobiotin agarose (Thermo Fisher Scientific, USA) according to manufacturer's
602 instructions.

603   To the tissue of wild type protonema, grounded in liquid nitrogen, the lysis buffer (PBS,
604 150 mM NaCl, 0,1% Triton X-100, 0,2% NP-40, Protease inhibitor cocktail for plant cell
605 extracts (Sigma)) was added. Lysate was incubated on ice for 30 min with rotation (Heidolph
606 Duomax 1030) and centrifuged 14 000g, 15 min, 4 C (Eppendorf Centrifuge 5418 R). 15 µg of
607 recombinant FAMOSS-streptavidin/streptavidin was added to supernatant and incubated 1h on
608 ice with rotation. Proteins in solution were cross-linked by 3 mM DSP (Thermo Fisher Scientific
609 Pierce) and incubated during 2 h. Reaction was quenched by 40 mM Tris-HCl pH 8 during 15
610 min on ice, then 50 mM ammonium bicarbonate was added. Samples were centrifuged at 14 000
611 g 10 min. The 20 mkl of pre-washed by washing buffer (50 mM ammonium bicarbonate-NaOH
612 pH 11, 500 mM NaCl, 0,1% Triton X-100, 0,2% NP-40) iminobiotin agarose (Thermo Fisher
613 Scientific Pierce) was added to supernatant and incubated on ice during 1h, washed 4 times by
614 washing buffer. Proteins of interest were eluted three times by 50 mM ammonium acetate pH3
615 with 500 mM NaCl. Eluates was neutralised by 20 mM Tris and clean-uped by Amicon Ultra-0.5
616 Centrifugal Filter Unit Ultracel-3K (Millipore). After that the crosslinker was cleaved with 20
617 mM DTT by heating at 50 C.

618 **Co-immunoprecipitation**

619   To identify the proteins which interact with FAMOSS peptide the co-immunoprecipitation
620 approach was used. The plant tissue, which was grounded at liquid nitrogen, was homogenized
621 in 450 mkl lysis buffer (50 mM Tris-HCl pH 8, 150 mM NaCl, 0,1% Tween-20, 10 mkl/ml
622 protease inhibitor cocktail (Sigma)). The resulting suspension was incubated on ice 30 min with
623 rotation and centrifuged at 13 000g for 15 min, 4 C (Eppendorf Centrifuge 5418 R). Proteins in
624 the clear supernatant (protein extract) were cross-linked with 5 mM DSP (Thermo Fisher
625 Scientific Pierce) for 2 h with agitation. The reaction was stopped with 40 mM Tris-HCl pH 8
626 during 15 min incubation. Samples were centrifuged at 14 000 g 10 min. The 50 µl pre-washed
627 with washing buffer (50 mM Tris-HCl pH 8, 150 mM NaCl, 0,1% Tween-20) M2 anti-FLAG

25

628   magnetic beads (Sigma) was added to supernatant. The samples were incubated 2 h on ice with

629   rotation of the washing buffer and once with 700 mkl of TBS (50 mM Tris-HCl pH 8, 150 mM

630   NaCl). The protein complexes were specifically eluted with 125 mkl of 100 ng/mkl 3xFLAG

631   peptide (Sigma) solution in TBS during 30 min on-ice incubation with agitation. The crosslinker

632   was cleaved with 20 mM DTT by heating at 50 C.

SDS-PAGE and in-gel trypsin digestion

634   Proteins after pull-down and Co-IP experiments were vacuum dried, dissolved in a sodium

635   dodecyl sulphate-polyacrylamide gel electrophoresis (SDS-PAGE) loading buffer (Bio-Rad) and

636   separated on 15 % SDS-PAGE gels following the Laemmli method (Laemmli, 1970). Gels were

637   stained as described previously (Schagger, 2006). The gel pieces corresponding 25 kDa MW

638   were cut, destained by 15 mM sodium thiosulfate and 50 mM potassium ferricyanide. Protein in-

639   gel trypsin digestion was conducted as described by (Rubtsova *et al.*, 2018).

Regeneration of protonema from protoplasts

641   Protoplast was prepared from protonemata as described previously (Fesenko et al., 2015)

642   and incubated during the 6 days on solid BCD agar medium. Regenerated protonema was

643   detected by microscopy analysis.

Fluorescent microscopy

645   To detect vesicles, protonemal cells were stained by the 5 µM of fluorescent dye

646   SynaptoGreen C4 (equivalent to FM1-43, Biotium, USA. SynaptoGreen C4 is a synonym of

647   fluorescent probe which is originally called FM1-43 dye and is available from Biotium under the

648   trademark name of SynaptoGreen™) during 5 min and washed. To visualize cell walls the

649   protonema cells were stained by 10 µg/mL of propidium iodide (fluorescein diacetate, Sigma-

650   Aldrich, USA) during 5 min. Fluorescence was detected by Axio Imager M2 microscope (Zeiss)

651   with an AxioCam 506 mono digital camera (Zeiss) and Zen 2.6 pro software (Zeiss). Filter unit

652   44 FITC (λex BP 475 nm/40 nm; λem BP 530 nm/50 nm) was used for SynaptoGreen C4

653   fluorescence detection, Filter unit 20 Rhodamin (λex BP 546/12 nm; λem BP 575–640 nm) was used

654   for propidium iodide.

Statistical analysis

656   Statistical analysis and visualisation were made in Python v. 3.7.5(Van Rossum, Drake,
657   1995) using modules scipy 1.5.2 (Virtanen et al., 2020), seaborn 0.11.1 (Waskom, 2021), numpy
658   1.20.1, pandas 1.2. 3 (McKinney, 2012).

Data availability

660   The mass spectrometry proteomic data have been deposited to the ProteomeXchange
661   Consortium via the PRIDE (Perez-Riverol et al., 2019) partner repository with the dataset
662   identifiers PXD028296 and PXD028342.

663

REFERENCES

1. Anderson, D.M., Anderson, K.M., Chang, C.L., Makarewich, C.A., Nelson, B.R., McAnally, J.R., Kasaragod, P., Shelton, J.M., Liou, J., Bassel-Duby, R., et al. (2015). A Micropeptide Encoded by a Putative Long Noncoding RNA Regulates Muscle Performance. Cell 160:595-606. 10.1016/j.cell.2015.01.009.

2. Aslanidis, C., and de Jong, P.J. (1990). Ligation-independent cloning of PCR products (LIC-PCR). Nucleic Acids Res 18:6069-6074. 10.1093/nar/18.20.6069.

3. Bailey, T.L., Johnson, J., Grant, C.E., and Noble, W.S. (2015). The MEME Suite. Nucleic Acids Res 43:W39-49. 10.1093/nar/gkv416.

4. Blanvillain, R., Young, B., Cai, Y.M., Hecht, V., Varoquaux, F., Delorme, V., Lancelin, J.M., Delseny, M., and Gallois, P. (2011). The Arabidopsis peptide kiss of death is an inducer of programmed cell death. Embo J 30:1173-1183. 10.1038/emboj.2011.14.

5. Bove, J., Vaillancourt, B., Kroeger, J., Hepler, P.K., Wiseman, P.W., Geitmann A. (2008) Magnitude and Direction of Vesicle Dynamics in Growing Pollen Tubes Using Spatiotemporal Image Correlation Spectroscopy and Fluorescence Recovery after Photobleaching. Plant Physiology 147:1646–1658. https://doi.org/10.1104/pp.108.120212

6. Brito, M.S., DePaoli, H.C., Cossalter, V., Avanci, N.C., Ferreira, P.B., Azevedo, M.S., Strini, E.J., Quiapim, A.C., Goldman, G.H., Peres, L.E.P., et al. (2018). A novel cysteine-rich peptide regulates cell expansion in the tobacco pistil and influences its final size. Plant science : an international journal of experimental plant biology 277:55-67. 10.1016/j.plantsci.2018.09.002.

7. Casson, S.A., Chilley, P.M., Topping, J.F., Evans, I.M., Souter, M.A., and Lindsey, K. (2002). The POLARIS gene of Arabidopsis encodes a predicted peptide required for correct root growth and leaf vascular patterning. The Plant cell 14:1705-1721. 10.1105/tpc.002618.

8. Castro, A., Vidal, S., and Ponce de Leon, I. (2016). Moss Pathogenesis-Related-10 Protein Enhances Resistance to Pythium irregulare in Physcomitrella patens and Arabidopsis thaliana. Front Plant Sci 7:580. 10.3389/fpls.2016.00580.

9. Chen, C., Heo, J.B. (2018) Overexpression of Constitutively Active OsRab11 in Plants Enhances Tolerance to High Salinity Levels. J. Plant Biol. 61:169-176. 10.1007/s12374-018-0048-0.

10. Chen, D., He, L., Lin, M., Jing, Y., Liang, C., Liu, H., Gao, J., Zhang, W., and Wang, M. (2021). A ras-related small GTP-binding protein, RabE1c, regulates stomatal movements

698　　　and drought stress responses by mediating the interaction with ABA receptors. Plant
699　　　science : an international journal of experimental plant biology 306:110858.
700　　　10.1016/j.plantsci.2021.110858.

701　11. Chen, Q.J., Deng, B.H., Gao, J., Zhao, Z.Y., Chen, Z.L., Song, S.R., Wang, L., Zhao,
702　　　L.P., Xu, W.P., Zhang, C.X., et al. (2020). A miRNA-Encoded Small Peptide, vvi-
703　　　miPEP171d1, Regulates Adventitious Root Formation. Plant Physiol 183:656-670.
704　　　10.1104/pp.20.00197.

705　12. Chng, S.C., Ho, L.N., Tian, J., and Reversade, B. (2013). ELABELA: A Hormone
706　　　Essential for Heart Development Signals via the Apelin Receptor. Dev Cell 27:672-680.
707　　　10.1016/j.devcel.2013.11.002.

708　13. Chugunova, A., Loseva, E., Mazin, P., Mitina, A., Navalayeu, T., Bilan, D.,
709　　　Vishnyakova, P., Marey, M., Golovina, A., Serebryakova, M., et al. (2019). LINC00116
710　　　codes for a mitochondrial peptide linking respiration and lipid metabolism. Proc Natl
711　　　Acad Sci U S A 116:4940-4945. 10.1073/pnas.1809105116.

712　14. Collonnier, C., Guyon-Debast, A., Maclot, F., Mara, K., Charlot, F., and Nogue, F.
713　　　(2017). Towards mastering CRISPR-induced gene knock-in in plants: Survey of key
714　　　features and focus on the model Physcomitrella patens. Methods 121-122:103-117.
715　　　10.1016/j.ymeth.2017.04.024.

716　15. Cove, D.J., Perroud, P.F., Charron, A.J., McDaniel, S.F., Khandelwal, A., and Quatrano,
717　　　R.S. (2009). Isolation of DNA, RNA, and protein from the moss Physcomitrella patens
718　　　gametophytes. Cold Spring Harb Protoc 2009:pdb prot5146. 10.1101/pdb.prot5146.

719　16. D'Lima, N.G., Ma, J., Winkler, L., Chu, Q., Loh, K.H., Corpuz, E.O., Budnik, B.A.,
720　　　Lykke-Andersen, J., Saghatelian, A., and Slavoff, S.A. (2017). A human microprotein
721　　　that interacts with the mRNA decapping complex. Nat Chem Biol 13:174-180.
722　　　10.1038/Nchembio.2249.

723　17. Dao, T.T., Linthorst, H.J., and Verpoorte, R. (2011). Chalcone synthase and its functions
724　　　in plant resistance. Phytochemistry reviews : proceedings of the Phytochemical Society
725　　　of Europe 10:397-412. 10.1007/s11101-011-9211-7.

726　18. De Rybel, B., van den Berg, W., Lokerse, A., Liao, C.Y., van Mourik, H., Moller, B.,
727　　　Peris, C.L., and Weijers, D. (2011). A versatile set of ligation-independent cloning
728　　　vectors for functional studies in plants. Plant Physiol 156:1292-1299.
729　　　10.1104/pp.111.177337.

730　19. Delwiche, C.F., and Cooper, E.D. (2015). The Evolutionary Origin of a Terrestrial Flora.
731　　　Current biology : CB 25:R899-910. 10.1016/j.cub.2015.08.029.

732 20. Dong, X., Wang, D., Liu, P., Li, C., Zhao, Q., Zhu, D., and Yu, J. (2013). Zm908p11,
733   encoded by a short open reading frame (sORF) gene, functions in pollen tube growth as a
734   profilin ligand in maize. J Exp Bot 64:2359-2372. 10.1093/jxb/ert093.

735 21. de Graaf, B.H.J., Cheung, A.Y., Andreyeva, T., Levasseur, K., Kieliszewski, M., Wu H.
736   (2005) Rab11 GTPase-Regulated Membrane Trafficking Is Crucial for Tip-Focused
737   Pollen Tube Growth in Tobacco. The Plant Cell 17: 2564–2579. 10.1105/tpc.105.033183.

738 22. Eaton D.A.R. (2020) Toytree: A minimalist tree visualization and manipulation library
739   for Python. Methods Ecol Evol. 11:187–191. 10.1111/2041-210X.13313.

740 23. Eddy, S.R. (2011). Accelerated Profile HMM Searches. PLoS Comput Biol 7:e1002195.
741   10.1371/journal.pcbi.1002195.

742 24. Elliott, L., Moore, I., Kirchhelle, C. (2020) Spatio-temporal control of post-Golgi
743   exocytic trafficking in plants. J Cell Sci 13: jcs237065.
744   https://doi.org/10.1242/jcs.237065

745 25. Faurobert, M., Pelpoir, E., and Chaib, J. (2007). Phenol extraction of proteins for
746   proteomic studies of recalcitrant plant tissues. Methods Mol Biol 355:9-14. 10.1385/1-
747   59745-227-0:9.

748 26. Fesenko I., Shabalina, S.A., Mamaeva, A., Knyazev, A., Glushkevich, A., Lyapina, I.,
749   Ziganshin, R., Kovalchuk, S., Kharlampieva, D., Lazarev, V., Taliansky, M., Koonin,
750   E.V. (2021) A vast pool of lineage-specific microproteins encoded by long non-coding
751   RNAs in plants. Nucleic Acids Research, https://doi.org/10.1093/nar/gkab816

752 27. Fesenko, I., Kirov, I., Kniazev, A., Khazigaleeva, R., Lazarev, V., Kharlampieva, D.,
753   Grafskaia, E., Zgoda, V., Butenko, I., Arapidi, G., et al. (2019). Distinct types of short
754   open reading frames are translated in plant cells. Genome Res 29:1464-1477.
755   10.1101/gr.253302.119.

756 28. Fesenko, I.A., Arapidi, G.P., Skripnikov, A.Y., Alexeev, D.G., Kostryukova, E.S.,
757   Manolov, A.I., Altukhov, I.A., Khazigaleeva, R.A., Seredina, A.V., Kovalchuk, S.I., et
758   al. (2015). Specific pools of endogenous peptides are present in gametophore, protonema,
759   and protoplast cells of the moss Physcomitrella patens. Bmc Plant Biol 15:87.
760   10.1186/s12870-015-0468-7.

761 29. Fujimoto, M., and Tsutsumi, N. (2014). Dynamin-related proteins in plant post-Golgi
762   traffic. Front Plant Sci 5:408. 10.3389/fpls.2014.00408.

763 30. Goodstein, D.M., Shu, S., Howson, R., Neupane, R., Hayes, R.D., Fazo, J., Mitros, T.,
764   Dirks, W., Hellsten, U., Putnam, N., et al. (2012). Phytozome: a comparative platform for
765   green plant genomics. Nucleic Acids Res 40:D1178-1186. 10.1093/nar/gkr944.

766   31. Guo, B., Wu, S., Zhu, X., Zhang, L., Deng, J., Li, F., Wang, Y., Zhang, S., Wu, R., Lu, J.,
767   et al. (2020). Micropeptide CIP2A-BP encoded by LINC00665 inhibits triple-negative
768   breast cancer progression. Embo J 39:e102190. 10.15252/embj.2019102190.

769   32. Hanada, K., Higuchi-Takeuchi, M., Okamoto, M., Yoshizumi, T., Shimizu, M.,
770   Nakaminami, K., Nishi, R., Ohashi, C., Iida, K., Tanaka, M., et al. (2013). Small open
771   reading frames associated with morphogenesis are hidden in plant genomes. Proceedings
772   of the National Academy of Sciences of the United States of America 110:2395-2400.
773   10.1073/pnas.1213958110.

774   33. Hoepflinger, M.C., Geretschlaeger, A., Sommer, A., Hoeftberger, M., Nishiyama, T.,
775   Sakayama, H., Hammerl, P., Tenhaken, R., Ueda, T., and Foissner, I. (2013). Molecular
776   and biochemical analysis of the first ARA6 homologue, a RAB5 GTPase, from green
777   algae. J Exp Bot 64:5553-5568. 10.1093/jxb/ert322.

778   34. Huang, J.Z., Chen, M., Chen, D., Gao, X.C., Zhu, S., Huang, H.Y., Hu, M., Zhu, H.F.,
779   and Yan, G.R. (2017). A Peptide Encoded by a Putative lncRNA HOXB-AS3 Suppresses
780   Colon Cancer Growth. Mol Cell 68:171-+. 10.1016/j.molcel.2017.09.015.

781   35. Ikeuchi, M., Yamaguchi, T., Kazama, T., Ito, T., Horiguchi, G., and Tsukaya, H. (2011).
782   ROTUNDIFOLIA4 regulates cell proliferation along the body axis in Arabidopsis shoot.
783   Plant Cell Physiol 52:59-69. 10.1093/pcp/pcq138.

784   36. Immarigeon, C., Frei, Y., Delbare, S.Y.N., Gligorov, D., Almeida, P.M., Grey, J.,
785   Fabbro, L., Nagoshi, E., Billeter, J.C., Wolfner, M.F., et al. (2021). Identification of a
786   micropeptide and multiple secondary cell genes that modulate Drosophila male
787   reproductive success. P Natl Acad Sci USA 118ARTN e2001897118

788   37. 10.1073/pnas.2001897118.

789   38. Jaeger, R., and Moody, L.A. (2021). A fundamental developmental transition in
790   Physcomitrium patens is regulated by evolutionarily conserved mechanisms. Evolution &
791   development 23:123-136. 10.1111/ede.12376.

792   39. Jang, G., and Dolan, L. (2011). Auxin promotes the transition from chloronema to
793   caulonema in moss protonema by positively regulating PpRSL1and PpRSL2 in
794   Physcomitrella patens. The New phytologist 192:319-327. 10.1111/j.1469-
795   8137.2011.03805.x.

796   40. Jelinkova, A., Malinska, K., Simon, S., Kleine-Vehn, J., Parezova, M., Pejchar, P.,
797   Kubes, M., Martinec, J., Friml, J., Zazimalova, E., et al. (2010). Probing plant
798   membranes with FM dyes: tracking, dragging or blocking? The Plant journal : for cell
799   and molecular biology 61:883-892. 10.1111/j.1365-313X.2009.04102.x.

800   41. Jilly, R., Khan, N.Z., Aronsson, H., and Schneider, D. (2018). Dynamin-Like Proteins
801   Are Potentially Involved in Membrane Dynamics within Chloroplasts and Cyanobacteria.
802   Front Plant Sci 9:206. 10.3389/fpls.2018.00206.

803   42. Jumper, J., Evans, R., Pritzel, A., Green, T., Figurnov, M., Ronneberger, O.,
804   Tunyasuvunakool, K., Bates, R., Zidek, A., Potapenko, A., et al. (2021). Highly accurate
805   protein structure prediction with AlphaFold. Nature 596:583-589. 10.1038/s41586-021-
806   03819-2.

807   43. Katoh, K., and Standley, D.M. (2013). MAFFT multiple sequence alignment software
808   version 7: improvements in performance and usability. Mol Biol Evol 30:772-780.
809   10.1093/molbev/mst010.

810   44. Krogh, A., Larsson, B., von Heijne, G., and Sonnhammer, E.L. (2001). Predicting
811   transmembrane protein topology with a hidden Markov model: application to complete
812   genomes. Journal of molecular biology 305:567-580. 10.1006/jmbi.2000.4315.

813   45. Kwon, C., Lee, J.H., and Yun, H.S. (2020). SNAREs in Plant Biotic and Abiotic Stress
814   Responses. Molecules and cells 43:501-508. 10.14348/molcells.2020.0007.

815   46. Laemmli, U.K. (1970). Cleavage of structural proteins during the assembly of the head of
816   bacteriophage T4. Nature 227:680-685. 10.1038/227680a0.

817   47. Lang, D., Ullrich, K.K., Murat, F., Fuchs, J., Jenkins, J., Haas, F.B., Piednoel, M.,
818   Gundlach, H., Van Bel, M., Meyberg, R., et al. (2018). The Physcomitrella patens
819   chromosome-scale assembly reveals moss genome structure and evolution. The Plant
820   journal : for cell and molecular biology 93:515-533. 10.1111/tpj.13801.

821   48. Li, H. (2016). Minimap and miniasm: fast mapping and de novo assembly for noisy long
822   sequences. Bioinformatics 32:2103-2110. 10.1093/bioinformatics/btw152.

823   49. Li, H., Handsaker, B., Wysoker, A., Fennell, T., Ruan, J., Homer, N., Marth, G.,
824   Abecasis, G., Durbin, R., and Genome Project Data Processing, S. (2009). The Sequence
825   Alignment/Map   format   and   SAMtools.   Bioinformatics   25:2078-2079.
826   10.1093/bioinformatics/btp352.

827   50. Li, L.J., Leng, R.X., Fan, Y.G., Pan, H.F., and Ye, D.Q. (2017). Translation of noncoding
828   RNAs: Focus on lncRNAs, pri-miRNAs, and circRNAs. Exp Cell Res 361:1-8.
829   10.1016/j.yexcr.2017.10.010.

830   51. Lycett, G. (2008). The role of Rab GTPases in cell wall metabolism. J Exp Bot 59:4061-
831   4074. 10.1093/jxb/ern255.

832   52. Ma, Q.-H. (2007) Small GTP-binding Proteins and their Functions in Plants. J Plant
833   Growth Regul 26:369–388.10.1007/s00344-007-9022-7.

32

834   53. Magny, E.G., Pueyo, J.I., Pearl, F.M.G., Cespedes, M.A., Niven, J.E., Bishop, S.A., and
835   Couso, J.P. (2013). Conserved Regulation of Cardiac Calcium Uptake by Peptides
836   Encoded in Small Open Reading Frames. Science 341:1116-1120.
837   10.1126/science.1238802.

838   54. MartiniEre, A., and Moreau, P. (2020). Complex roles of Rabs and SNAREs in the
839   secretory pathway and plant development: a never-ending story. J Microsc 280:140-157.
840   10.1111/jmi.12952.

841   55. Matsumoto, A., Pasut, A., Matsumoto, M., Yamashita, R., Fung, J., Monteleone, E.,
842   Saghatelian, A., Nakayama, K.I., Clohessy, J.G., and Pandolfi, P.P. (2017). mTORC1
843   and muscle regeneration are regulated by the LINC00961-encoded SPAR polypeptide.
844   Nature 541:228-232. 10.1038/nature21034.

845   56. McKinney,W. (2012) Python for Data Analysis: Data Wrangling with Pandas, NumPy,
846   and IPython 'O'Reilly Media, Inc.'.

847   57. Mellacheruvu, D., Wright, Z., Couzens, A.L., Lambert, J.P., St-Denis, N.A., Li, T.,
848   Miteva, Y.V., Hauri, S., Sardiu, M.E., Low, T.Y., et al. (2013). The CRAPome: a
849   contaminant repository for affinity purification-mass spectrometry data. Nature methods
850   10:730-736. 10.1038/nmeth.2557.

851   58. Minamino, N., and Ueda, T. (2019). RAB GTPases and their effectors in plant endosomal
852   transport. Current opinion in plant biology 52:61-68. 10.1016/j.pbi.2019.07.007.

853   59. Nguyen, L.T., Schmidt, H.A., von Haeseler, A., and Minh, B.Q. (2015). IQ-TREE: a fast
854   and effective stochastic algorithm for estimating maximum-likelihood phylogenies. Mol
855   Biol Evol 32:268-274. 10.1093/molbev/msu300.

856   60. Nishiyama, T., Sakayama, H., de Vries, J., Buschmann, H., Saint-Marcoux, D., Ullrich,
857   K.K., Haas, F.B., Vanderstraeten, L., Becker, D., Lang, D., et al. (2018). The Chara
858   Genome: Secondary Complexity and Implications for Plant Terrestrialization. Cell
859   174:448-464 e424. 10.1016/j.cell.2018.06.033.

860   61. Niu, L., Lou, F., Sun, Y., Sun, L., Cai, X., Liu, Z., Zhou, H., Wang, H., Wang, Z., Bai, J.,
861   et al. (2020). A micropeptide encoded by lncRNA MIR155HG suppresses autoimmune
862   inflammation via modulating antigen presentation. Science advances 6:eaaz2059.
863   10.1126/sciadv.aaz2059.

864   62. Notredame, C., Higgins, D.G., and Heringa, J. (2000). T-Coffee: A novel method for fast
865   and accurate multiple sequence alignment. Journal of molecular biology 302:205-217.
866   10.1006/jmbi.2000.4042.

867   63. One Thousand Plant Transcriptomes, I. (2019). One thousand plant transcriptomes and
868   the phylogenomics of green plants. Nature 574:679-685. 10.1038/s41586-019-1693-2.

64. Orr, R.G., Cheng, X., Vidali, L., and Bezanilla, M. (2020). Orchestrating cell morphology from the inside out - using polarized cell expansion in plants as a model. Current opinion in cell biology 62:46-53. 10.1016/j.ceb.2019.08.004.

65. Orr, R.G., Furt, F., Warner, E.L., Agar, E.M., Garbarino, J.M., Cabral, S.E., Dubuke, M.L., Butt, A.M., Munson, M., and Vidali, L. (2021). Rab-E and its interaction with myosin XI are essential for polarised cell growth. The New phytologist 229:1924-1936. 10.1111/nph.17023.

66. Ovecka, M., Berson, T., Beck, M., Derksen, J., Samaj, J., Baluska, F., and Lichtscheidl, I.K. (2010). Structural sterols are involved in both the initiation and tip growth of root hairs in Arabidopsis thaliana. The Plant cell 22:2999-3019. 10.1105/tpc.109.069880.

67. Ow, S.Y., Salim, M., Noirel, J., Evans, C., Rehman, I., and Wright, P.C. (2009). iTRAQ underestimation in simple and complex mixtures: "the good, the bad and the ugly". J Proteome Res 8:5347-5355. 10.1021/pr900634c.

68. Paniagua, C., Bilkova, A., Jackson, P., Dabravolski, S., Riber, W., Didi, V., Houser, J., Gigli-Bisceglia, N., Wimmerova, M., Budinska, E., et al. (2017). Dirigent proteins in plants: modulating cell wall metabolism during abiotic and biotic stress exposure. J Exp Bot 68:3287-3301. 10.1093/jxb/erx141.

69. Peaucelle, A., Braybrook, S.A., Le Guillou, L., Bron, E., Kuhlemeier, C., and Hofte, H. (2011). Pectin-induced changes in cell wall mechanics underlie organ initiation in Arabidopsis. Current biology : CB 21:1720-1726. 10.1016/j.cub.2011.08.057.

70. Perez-Riverol, Y., Csordas, A., Bai, J., Bernal-Llinares, M., Hewapathirana, S., Kundu, D.J., Inuganti, A., Griss, J., Mayer, G., Eisenacher, M., et al. (2019) The PRIDE database and related tools and resources in 2019: improving support for quantification data. Nucleic Acids Res. 47: D442–D450.

71. Pleskot, R., Pejchar, P., Bezvoda, R., Lichtscheidl, I.K., Wolters-Arts, M., Marc, J., Žárský, V., Potocký, M. (2012). Turnover of phosphatidic acid through distinct signaling pathways affects multiple aspects of pollen tube growth in tobacco. Frontiers in plant science 3:1-13.

72. Polycarpou-Schwarz, M., Gross, M., Mestdagh, P., Schott, J., Grund, S.E., Hildenbrand, C., Rom, J., Aulmann, S., Sinn, H.P., Vandesompele, J., et al. (2018). The cancer-associated microprotein CASIMO1 controls cell proliferation and interacts with squalene epoxidase modulating lipid droplet formation. Oncogene 37:4750-4768. 10.1038/s41388-018-0281-5.

73. Preuss, M.L., Serna, J., Falbel, T.G., Bednarek, S.Y., and Nielsen, E. (2004). The Arabidopsis Rab GTPase RabA4b localizes to the tips of growing root hair cells. The Plant cell 16:1589-1603. 10.1105/tpc.021634.

74. Rawat, A., Brejskova, L., Hala, M., Cvrckova, F., and Zarsky, V. (2017). The Physcomitrella patens exocyst subunit EXO70.3d has distinct roles in growth and development, and is essential for completion of the moss life cycle. The New phytologist 216:438-454. 10.1111/nph.14548.

75. Rensing, S.A., Goffinet, B., Meyberg, R., Wu, S.Z., and Bezanilla, M. (2020). The Moss Physcomitrium (Physcomitrella) patens: A Model Organism for Non-Seed Plants. The Plant cell 32:1361-1376. 10.1105/tpc.19.00828.

76. Rohrig, H., Schmidt, J., Miklashevichs, E., Schell, J., and John, M. (2002). Soybean ENOD40 encodes two peptides that bind to sucrose synthase. Proc Natl Acad Sci U S A 99:1915-1920. 10.1073/pnas.022664799.

77. Rounds, C.M., and Bezanilla, M. (2013). Growth mechanisms in tip-growing plant cells. Annual review of plant biology 64:243-265. 10.1146/annurev-arplant-050312-120150.

78. Rubtsova, M., Naraykina, Y., Vasilkova, D., Meerson, M., Zvereva, M., Prassolov, V., Lazarev, V., Manuvera, V., Kovalchuk, S., Anikanov, N., et al. (2018). Protein encoded in human telomerase RNA is involved in cell protective pathways. Nucleic Acids Res 46:8966-8977. 10.1093/nar/gky705.

79. Sabovljevic, M., Vujicic, M., Sabovljevic A. (2014). Plant growth regulators in bryophytes. Botanica serbica 38:99-107.

80. Samaj, J., Read, N.D., Volkmann, D., Menzel, D., Baluška, F. (2005) The endocytic network in plants. Trends in Cell Biology 15: 425-433. https://doi.org/10.1016/j.tcb.2005.06.006

81. Schagger, H. (2006). Tricine-SDS-PAGE. Nat Protoc 1:16-22. 10.1038/nprot.2006.4.

82. Singh, A., Vivek, A.T., and Kumar, S. (2021). AlnC: An extensive database of long non-coding RNAs in angiosperms. Plos One 16:e0247215. 10.1371/journal.pone.0247215.

83. Singh, U., and Wurtele, E.S. (2021). orfipy: a fast and flexible tool for extracting ORFs. Bioinformatics 10.1093/bioinformatics/btab090.

84. Slavoff, S.A., Heo, J.H., Budnik, B.A., Hanakahi, L.A., and Saghatelian, A. (2014). A Human Short Open Reading Frame (sORF)-encoded Polypeptide That Stimulates DNA End Joining. J Biol Chem 289:10950-10957. 10.1074/jbc.C113.533968.

85. Spechenkova, N., Fesenko, I.A., Mamaeva, A., Suprunova, T.P., Kalinina, N.O., Love, A.J., and Taliansky, M. (2021). The Resistance Responses of Potato Plants to Potato

936   Virus Y Are Associated with an Increased Cellular Methionine Content and an Altered
937   SAM:SAH Methylation Index. Viruses 1310.3390/v13060955.

938 86. Steger, M., Diez, F., Dhekne, H.S., Lis, P., Nirujogi, R.S., Karayel, O., Tonelli, F.,
939   Martinez, T.N., Lorentzen, E., Pfeffer, S.R., Alessi D.R., Mann, M. (2017) Systematic
940   proteomic analysis of LRRK2-mediated Rab GTPase phosphorylation establishes a
941   connection to ciliogenesis. eLife 6:e31012 DOI: 10.7554/eLife.31012

942 87. Stenzel, I., Hause, B., Miersch, O., Kurz, T., Maucher, H., Weichert, H., Ziegler, J.,
943   Feussner, I., and Wasternack, C. (2003). Jasmonate biosynthesis and the allene oxide
944   cyclase family of Arabidopsis thaliana. Plant Mol Biol 51:895-911.
945   10.1023/a:1023049319723.

946 88. Stevenson, S.R., Kamisugi, Y., Trinh, C.H., Schmutz, J., Jenkins, J.W., Grimwood, J.,
947   Muchero, W., Tuskan, G.A., Rensing, S.A., Lang, D., et al. (2016). Genetic Analysis of
948   Physcomitrella patens Identifies ABSCISIC ACID NON-RESPONSIVE, a Regulator of
949   ABA Responses Unique to Basal Land Plants and Required for Desiccation Tolerance.
950   The Plant cell 28:1310-1327. 10.1105/tpc.16.00091.

951 89. Szczesniak, M.W., Rosikiewicz, W., and Makalowska, I. (2016). CANTATAdb: A
952   Collection of Plant Long Non-Coding RNAs. Plant Cell Physiol 57:e8.
953   10.1093/pcp/pcv201.

954 90. Szumlanski, A.L., and Nielsen, E. (2009). The Rab GTPase RabA4d regulates pollen
955   tube tip growth in Arabidopsis thaliana. The Plant cell 21:526-544.
956   10.1105/tpc.108.060277.

957 91. Tavormina, P., De Coninck, B., Nikonorova, N., De Smet, I., and Cammue, B.P. (2015).
958   The Plant Peptidome: An Expanding Repertoire of Structural Features and Biological
959   Functions. The Plant cell 27:2095-2118. 10.1105/tpc.15.00440.

960 92. Thelander, M., Landberg, K., and Sundberg, E. (2018). Auxin-mediated developmental
961   control in the moss Physcomitrella patens. J Exp Bot 69:277-290. 10.1093/jxb/erx255.

962 93. Thorvaldsdottir, H., Robinson, J.T., and Mesirov, J.P. (2013). Integrative Genomics
963   Viewer (IGV): high-performance genomics data visualization and exploration. Brief
964   Bioinform 14:178-192. 10.1093/bib/bbs017.

965 94. Tran, L.T., Taylor, J.S., and Constabel, C.P. (2012). The polyphenol oxidase gene family
966   in land plants: Lineage-specific duplication and expansion. Bmc Genomics 13:395.
967   10.1186/1471-2164-13-395.

968 95. Vakirlis, N., Acar, O., Hsu, B., Castilho Coelho, N., Van Oss, S.B., Wacholder, A.,
969   Medetgul-Ernar, K., Bowman, R.W., 2nd, Hines, C.P., Iannotta, J., et al. (2020). De novo

36

970   emergence of adaptive membrane proteins from thymine-rich genomic sequences. Nat

971   Commun 11:781. 10.1038/s41467-020-14500-z.

972 96. van Gisbergen, P., Wu, S.-Z., Cheng, X., Pattavina, K.A., Bezanilla, M. (2020) In vivo

973   analysis of formin dynamics in the moss P. patens reveals functional class diversification.

974   J Cell Sci 133: jcs233791. https://doi.org/10.1242/jcs.233791

975 97. Van Rossum,G., Drake,F.L.,Jr (1995) Python tutorial Centrum voor Wiskunde en

976   Informatica Amsterdam.

977 98. Vidali, L., and Bezanilla, M. (2012). Physcomitrella patens: a model for tip cell growth

978   and differentiation. Current opinion in plant biology 15:625-631.

979   10.1016/j.pbi.2012.09.008.

980 99. Virtanen, P., Gommers, R., Oliphant, T.E., Haberland, M., Reddy, T., Cournapeau, D.,

981   Burovski, E., Peterson, P., Weckesser, W., Bright, J., et al. (2020). SciPy 1.0:

982   fundamental algorithms for scientific computing in Python. Nature methods 17:261-272.

983   10.1038/s41592-019-0686-2.

984 100.   Wang, X., Zhang, H., Gao, Y., Sun, G., Zhang, W., and Qiu, L. (2014). A

985   comprehensive analysis of the Cupin gene family in soybean (Glycine max). Plos One

986   9:e110092. 10.1371/journal.pone.0110092.

987 101.   Waskom,M. (2021) seaborn: statistical data visualization. J. Open Source Softw.,

988   6:3021.

989 102.   Ye, J., Coulouris, G., Zaretskaya, I., Cutcutache, I., Rozen, S., and Madden, T.L.

990   (2012). Primer-BLAST: a tool to design target-specific primers for polymerase chain

991   reaction. Bmc Bioinformatics 13:134. 10.1186/1471-2105-13-134.

Figure legends

Figure 1. FAMOSS is a widely conserved plant smORF-encoded peptide.

A - Sashimi plot showing *FAMOSS* transcription as confirmed using nanopore RNA sequencing in *Physcomitrium patens* protonema and gametophores. B - Construction of FAMOSS coupled with a GUS reporter protein at the FAMOSS promoter. Black arrows indicate primers used for identification. C, D - GUS staining of the protonema (C, scale bar = 200 μm) and gametophores (D, scale bar = 1 mm). E - The alignment of the FAMOSS peptide and orthologous sequences from different plants. F - Phylogenomic tree of the identified FAMOSS orthologs. Mosses, burgundy; liverworts, blue; algae, red; ferns, gray; gymnosperms, orange; angiosperms, green. G - *P. patens* FAMOSS structure and structures of its orthologs, predicted using AlphaFold.

Figure 2. The growth of mutant lines in different conditions.

A - The ratios of the two types of moss protonema filaments, caulonemata and chloronemata, in wild-type, *FAMOSS*-overexpressing (OE), and knockout (KO) plants. B - The lengths of the apical, first subapical, and second subapical cells. C - The effect of 6-benzylaminopurine (BAP) on protonemal morphology. Scale bar = 1 mm. D – The effect of abscisic acid (ABA) on protonemal morphology. E - The effect of BAP on the protonemal growth rate. F - The effect of ABA on protonemal growth. G - The effect of medium composition on protonemal growth. +G+AT, BCD medium supplemented with glucose and ammonium tartrate; +G−AT, BCD medium with glucose but without ammonium tartrate. H – Fold change (FC) in *FAMOSS* transcription after treatments with ABA, BAP, and indole-3-acetic acid (IAA). I, J - Quantitative proteomic analysis of the *FAMOSS*-overexpressing (OE) and knockout (KO) plants. Volcano plots of the entire set of proteins quantified in the iTRAQ analysis in the *FAMOSS* OE (I) and KO (J) lines. Proteins with significant differences in abundance relative to the wild type are depicted in color. GSA, glutamate-1-semialdehyde 2,1-aminomutase; rbfA, ribosome-binding factor A; RPS20, ribosomal protein S20; RPS30, ribosomal protein S30; AOC, allene oxide cyclase; GST, glutathione *S*-transferase; CHS, chalcone synthase; XTH, xyloglucan endotransglucosylase/hydrolase protein 23; PME, pectin methylesterase; rbcL, ribulose-1,5-bisphosphate carboxylase/oxygenase large subunit; GAPDH, glyceraldehyde-3-phosphate dehydrogenase A chloroplastic-like isoform X2; JAL3, jacalin-related lectin 3; PPO, polyphenol oxidase; PAL, phenylalanine ammonia-lyase; PR10, pathogenesis-related protein; PR10-like, pathogenesis-related protein-like; DIR, dirigent protein; SNAP25, synaptosomal-associated protein 25; ASPL, tether containing UBX

38

1026   domain for GLUT4; DRP1, dynamin-related protein 1E; CLTA, clathrin light chain; PYL5,

1027   pyrobactin resistance 1-like 5; PMM, phosphomannomutase; SSU, ribulose-1,5-bisphosphate

1028   carboxylase/oxygenase small subunits; DUF1955, domain of unknown function.

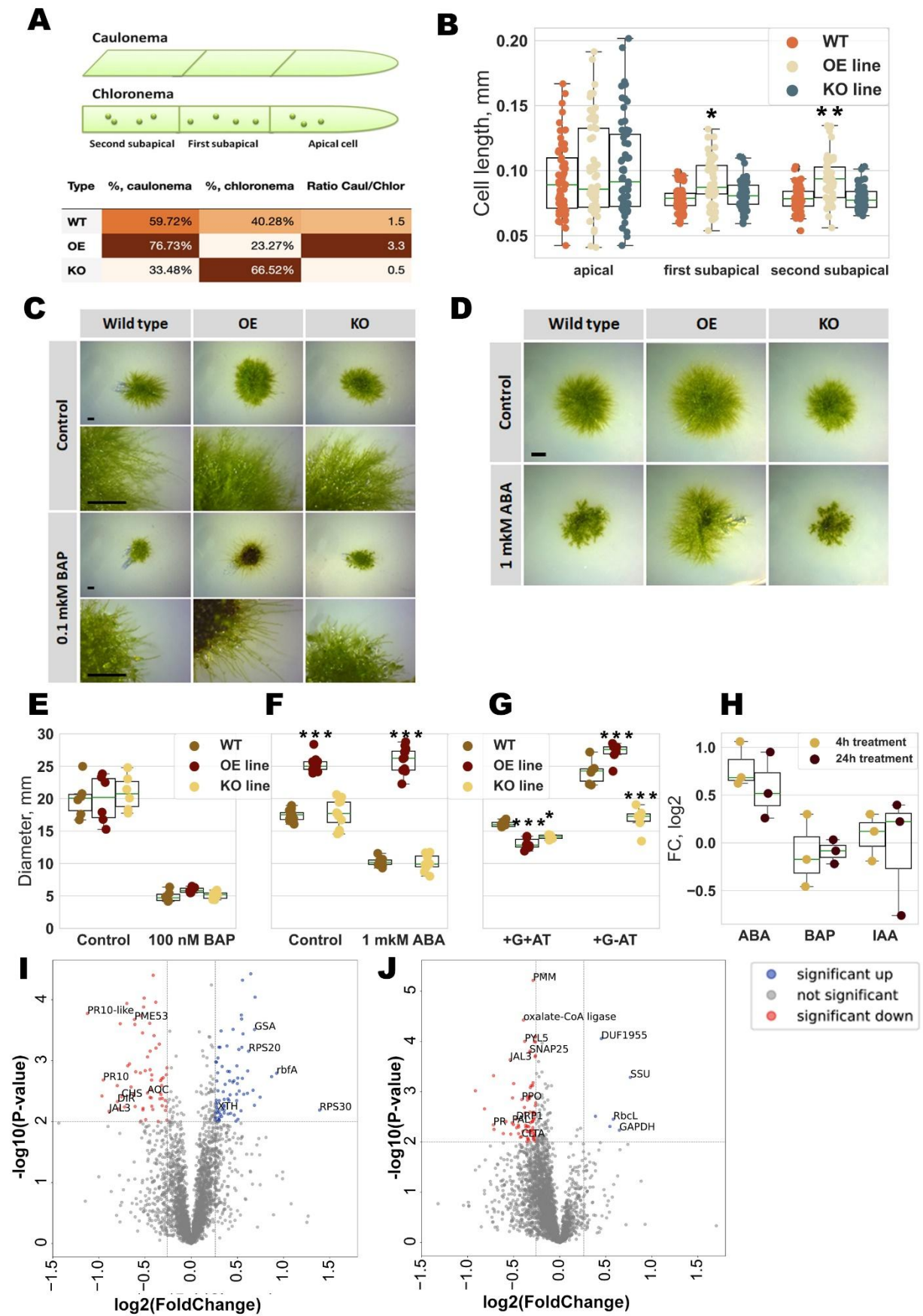1029   *, $P < 0.05$; **, $P < 0.01$; ***, $P < 0.001$.

1030   **Figure 4.** The growth rate of the mutant lines under stress-related conditions. A - Effect of

1031   NaCl on protonemal growth. B - Effect of paraquat (PQ) on protonemal growth. C - Effect of

1032   NaCl and PQ on protonemal morphology after 30 days of cultivation. D - *FAMOSS*

1033   expression under different stresses. *, $P < 0.05$; ***, $P < 0.001$.

1034   **Figure 5.** Analysis of the protein partners of the FAMOSS peptide. A - Diagram of the

1035   interactome experiments. B - Sequence and coverage of the FLAG-tagged FAMOSS

1036   sequence. C - Sequence of streptavidin (SAV)-tagged FAMOSS. D - Rab GTPases present in

1037   the two types of interactome experiments. Proteins detected in samples are marked with a

1038   plus sign, and those not detected are indicated with a minus sign. E − Alignment of Rab

1039   GTPases found in the FAMOSS interactomes.

1040

1041   **Figure 6.** The FAMOSS peptide affects vesicular trafficking. A–C - Apical protonemal cells

1042   stained with SynaptoGreen C4. (A − *FAMOSS*-overexpression line (OE); B − The wild type;

1043   C - *FAMOSS* knockout line (KO). D - Profile of SynaptoGreen C4 fluorescence in the apical

1044   cells. E - Boxplot showing the ratios of intensity of SynaptoGreen C4 staining at the distance

1045   15 mkm from the cell tip to the maximal intensity. ***, $P < 0.001$.
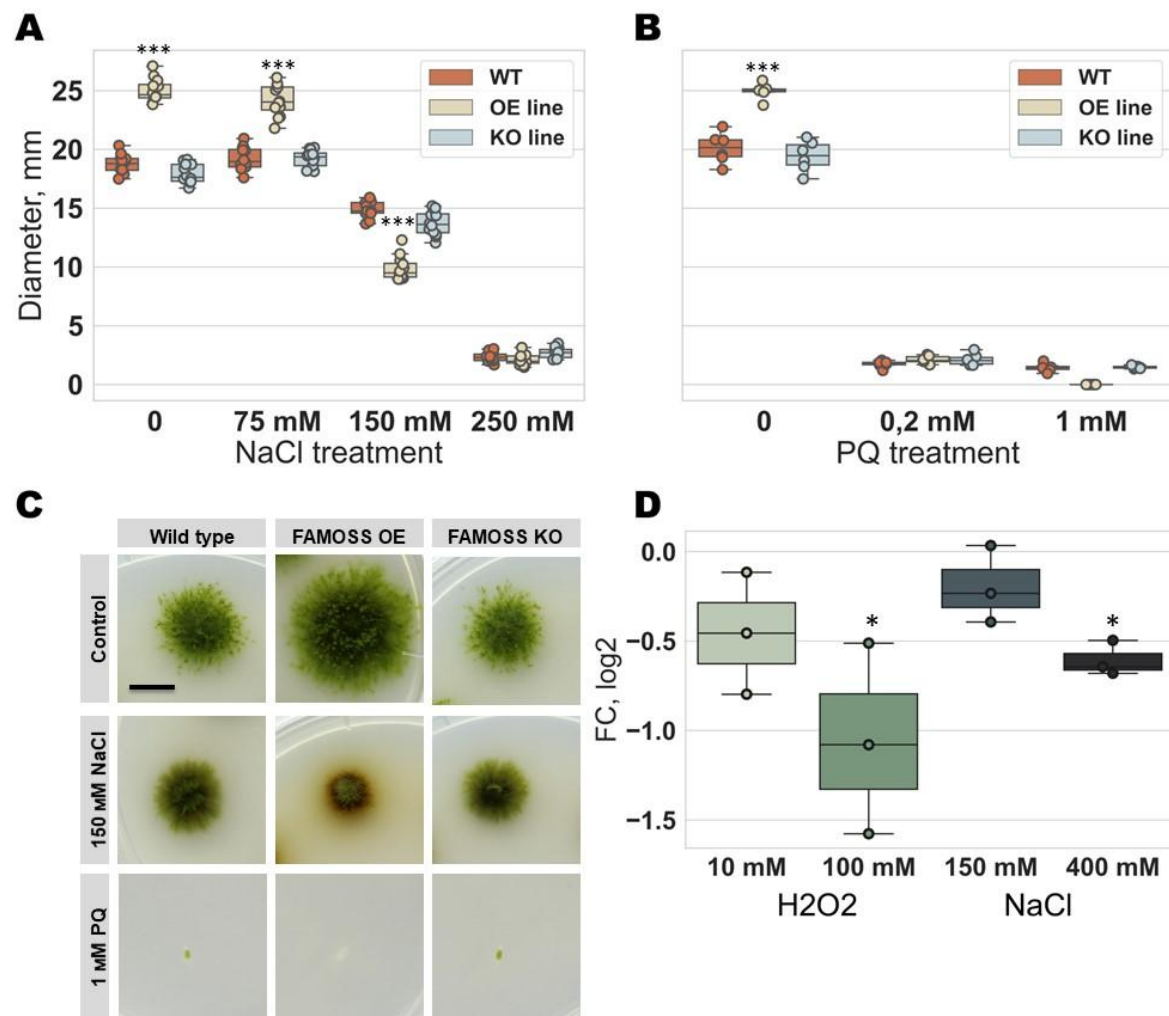
1046

1047   **Figure 7.** The mechanism of the regulation of plant physiological processes by the FAMOSS

1048   peptide. *FAMOSS* is expressed in favorable conditions and modulates the Rab signaling

1049   pathway to influence vesicular trafficking and ABA signaling. These processes increase

1050   protonemal growth, translation, and caulonemal formation, but decrease the ABA response

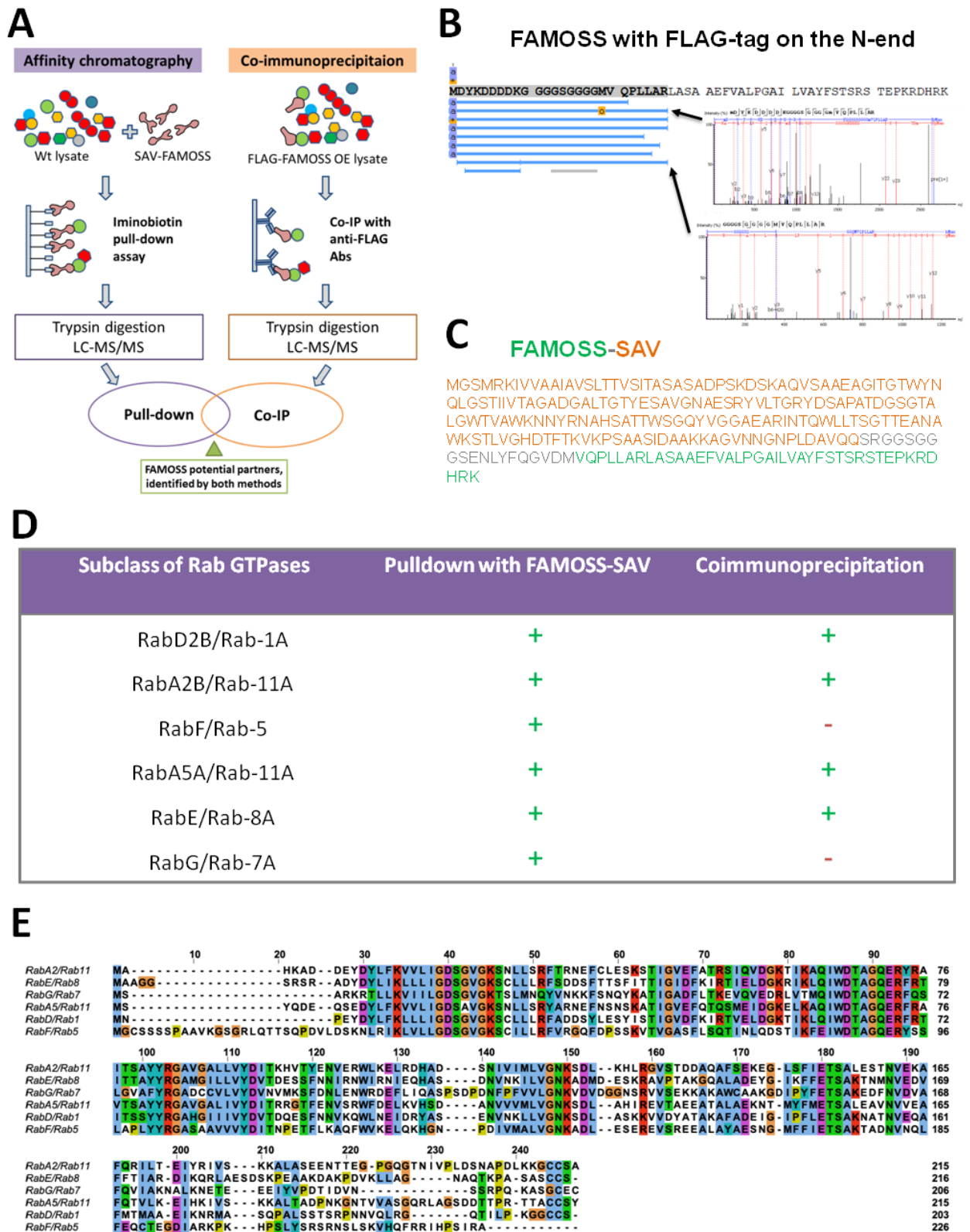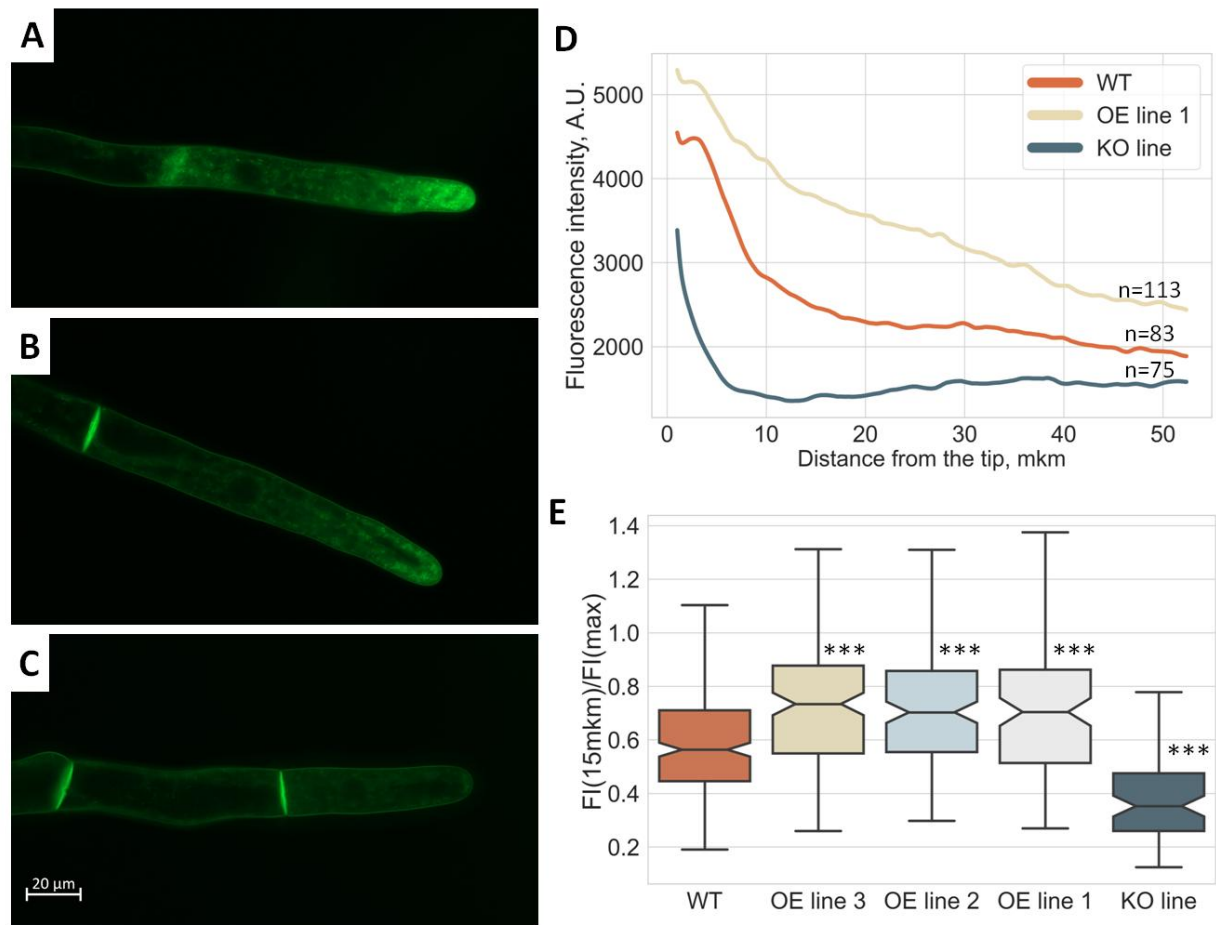1051   and, thus, the adaptability to stresses.

1052

Figures

1053

1054

1055   **Figure 1.**

1056

1057

1058 **Figure 2.**

1059

1060 **Figure 3.**

1061

1062   **Figure 4.**

1063

1064

1065   **Figure 5.**